Arc Control Experiments
Using a High Performance Arc Heater

J. H. Painter
McDonnell Douglas Astronautics Company—St. Louis Division
Saint Louis, Missouri 63166

October 1981

Final Report for Period 1 September 1980 — 30 June 1981

TECHNICAL REPORTS
FILE COPY

ARNOLD ENGINEERING DEVELOPMENT CENTER
ARNOLD AIR FORCE STATION, TENNESSEE
AIR FORCE SYSTEMS COMMAND
UNITED STATES AIR FORCE

This final report was submitted by McDonnell Douglas Astronautics Company—St. Louis Arc Heater Laboratory, St. Louis, Missouri, under contract number F40600-80-C-0005, with the Arnold Engineering Development Center (AEDC), Air Force Systems Command (AFSC), Arnold Air Force Station, Tennessee. Mr. Ross Roepke, AEDC/DOT was the Project Manager.

This report has been reviewed by the Office of Public Affairs (PA) and is releasable to the National Technical Information Service (NTIS). At NTIS, it will be available to the general public, including foreign nations.

APPROVAL STATEMENT

This report has been reviewed and approved.

ROSS G. ROEPKE
Directorate of Technology
Deputy for Operations

Approved for publication:

FOR THE COMMANDER

MARION L. LASTER
Director of Technology
Deputy for Operations

REPORT DOCUMENTATION PAGE		READ INSTRUCTIONS BEFORE COMPLETING FORM
1. REPORT NUMBER AEDC-TR-81-20	2. GOVT ACCESSION NO.	3. RECIPIENT'S CATALOG NUMBER
4. TITLE (and Subtitle) ARC CONTROL EXPERIMENTS USING A HIGH PERFORMANCE ARC HEATER		5. TYPE OF REPORT & PERIOD COVERED Final – 1 Sept. 1980 – 30 June 1981
		6. PERFORMING ORG. REPORT NUMBER
7. AUTHOR(s) J. H. Painter, McDonnell Douglas Astronautics Co., St. Louis Division		8. CONTRACT OR GRANT NUMBER(s) F40600-80-C-0005
9. PERFORMING ORGANIZATION NAME AND ADDRESS McDonnell Douglas Astronautics Company P.O. Box 516 St. Louis, MO 63166		10. PROGRAM ELEMENT, PROJECT, TASK AREA & WORK UNIT NUMBERS Program Element 65807F
11. CONTROLLING OFFICE NAME AND ADDRESS Arnold Engineering Development Center/DOS Air Force Systems Command Arnold Air Force Station, TN 37389		12. REPORT DATE October 1981
		13. NUMBER OF PAGES 78
14. MONITORING AGENCY NAME & ADDRESS(if different from Controlling Office)		15. SECURITY CLASS. (of this report) UNCLASSIFIED
		15a. DECLASSIFICATION/DOWNGRADING SCHEDULE N/A

16. DISTRIBUTION STATEMENT (of this Report)

Approved for public release; distribution unlimited.

17. DISTRIBUTION STATEMENT (of the abstract entered in Block 20, if different from Report)

18. SUPPLEMENTARY NOTES

Available in Defense Technical Information Center (DTIC).

19. KEY WORDS (Continue on reverse side if necessary and identify by block number)

arc heaters	electric arcs
test facilities	electrode phenomena
arc control	arc stability

20. ABSTRACT (Continue on reverse side if necessary and identify by block number)

Arc control experiments using a high performance arc heater have been conducted to evaluate and improve methods for controlling a high-pressure, high current arc. Arc control parameters varied in these experiments were: arc current, arc pressure, air flow rate, starting ramp rate, arc polarity, component resistance to ground, spin coil current, and gas injection distribution. Geometric parameters varied were: nozzle throat area, constrictor length,

DD FORM 1473 1 JAN 73 EDITION OF 1 NOV 65 IS OBSOLETE UNCLASSIFIED

20. ABSTRACT (Continued)

and gas injection radius. Arc characteristics were documented
on high-speed motion picture film at rates to 10,800 frames per
second and by oscillograph. Analysis of these data indicated
all of the parameters investigated had an effect on arc behavior
and these effects are documented herein. The role of gas cir-
culation and internal magnetic fields dominated other variations
of the control parameters. Reduction of the nozzle throat area
by a factor of two had a strong influence on the circulation
level and arc instabilities resulted.

Intersegment arcing was photographed at high frame rates as were
other arc instabilities such as blow-through, roll-over, and
kinking. Methods of improving the arc control and stability were
identified and evaluated within the scope of the program. A
total of 50 arc heater tests were made at arc currents to 830 A
and pressures to 50 atm.

PREFACE

The work reported herein was conducted by the McDonnell Douglas Astronautics Company-St. Louis (MDAC-STL) Arc Heater Laboratory, St. Louis, Missouri, for the Arnold Engineering Development Center (AEDC), Air Force Systems Command, under Contract F40600-80-C-0005, from 1 September 1980 to 30 June 1981. The AEDC Technical Representative was Mr. Ross Roepke.

The author wishes to acknowledge the contributions and assistance of the following persons whose help was instrumental in performing the work reported herein: Mr. Ross Roepke, AEDC; Mr. Dennis Horn, Calspan Corp.; Mr. John Bomar, Mr. James Grace, Mr. Wayne Mayden and Mr. Ron Williamson, MDAC-STL.

This technical report has been approved by W. A. Rinehart, Branch Chief, R. V. Masek, Chief Technology Engineer, and J. W. Twombly, Jr., Director Engineering Technology, MDAC-STL.

The reproducibles used in the reproduction of this report were supplied by the author.

CONTENTS

LIST OF ILLUSTRATIONS

LIST OF ILLUSTRATIONS (continued)

LIST OF TABLES

1.0   INTRODUCTION

Although significant advances in arc control have been made in recent years, present day arc heaters used in entry simulation facilities still encounter major arc instabilities that degrade performance and can cause severe and expensive hardware damage.[1-4]   This is particularly (although not uniquely) true for high arc pressures where the arc column voltage gradients are quite high and turbulence is present in the gas flow.   Poor location of the arc terminations, intercomponent arc-over, arc blow-through and severe arc kinking are but a few of the arc control problems being encountered.

The objective of this work was to conduct experiments using a high performance arc heater (HIPERARC) to evaluate and improve methods for controlling high pressure, high current arcs.   The experiments included variations of eight arc control parameters and three geometry factors.

Evaluation of arc control methods requires accurate documentation of the independent effects of each control parameter.   Such documentation has generally been restricted to overall heater performance and the net effect on hardware.   These experiments utilized high speed motion pictures combined with high speed oscillograph records to document high pressure arc characteristics while semi-independent and/or independent variations of the control parameters were made.

Analysis of the data from these experiments required viewing more than 300,000 frames of arc data and correlating that information with 50 oscillograph traces.   The results of the initial analysis is contained in this report.   Further analysis of the acquired data will add to the understanding of arc phenomena and it is anticipated that future work will glean even more information from these data than have been recovered to date.

This report describes the experimental apparatus, the experiments conducted, and the effects of the arc control variations.

2.0 EXPERIMENTAL APPARATUS

All of the experiments conducted under this program utilized a high performance arc heater (HIPERARC) exhausting to the test cabin of the MDAC Large Core Arc Tunnel (LCAT). The arc heater performance and arc characteristics were monitored using one or more high speed cameras, standard instrumentation and a color television camera.

2.1 HIGH PERFORMANCE ARC HEATER (HIPERARC)

The HIPERARC heater (Fig. 1) was designed to investigate flow phenomena in high performance arc heaters.[3] A toroidal shaped rear electrode (usually the anode) is separated from a diverging quarter-torus forward electrode by multiple isolated interelectrode segments. The entrance segments are curved and tapered to form the converger module followed by constant internal diameter segments in the constrictor. The constrictor length can be varied by adding modules of twelve segments or by adding individual segments. Each segment in the constrictor is 0.25 in. thick. The flow is accelerated downstream of the forward electrode by a converging-diverging nozzle to low supersonic speeds. The arc chamber is closed in the rear by two isolators and a rear shell.

All of the tests in this program were conducted using uncooled constrictor and converger segments. Thus, the test times were limited to less than three seconds. All other components were water-cooled. Two different nozzles were used. The first had a throat diameter of 0.53 in. and the second 0.375 in. Two different constrictor lengths were tested. The first contained two modules and the second had one module of twelve segments each.

The internal diameter of the rear isolators was 3 in. and the constrictor diameter was 0.9 in. The minimum diameter of the rear electrode was 1.5 in. The length from the mid-plane of the rear electrode to the entrance of the forward electrode was varied from 6.75 to 10.07 in.

Air was injected into the heater at each component interface from the first rear isolator to the nozzle. All air injected upstream of the constrictor was considered primary flow and all downstream of that point was considered secondary flow. An in-depth discussion of the gas injection is in Section 4.1.

11−3211
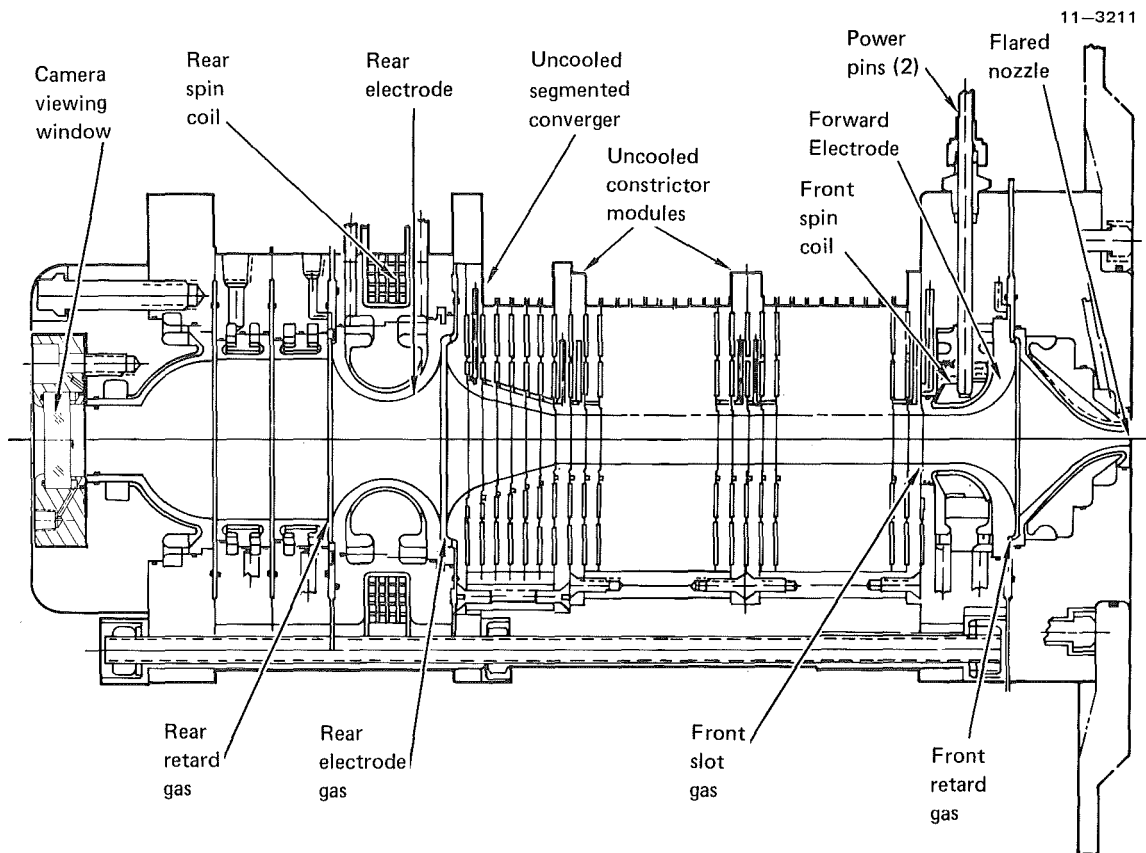
Figure 1   High performance arc heater (HIPERARC)

Figure 2 shows the HIPERARC as used in these experiments. The copper constrictor and converger segments can be seen in between the electrode housings. This photo shows only one constrictor module. The outer retaining bolts are isolated from all components with the white Delrin boots.

The forward electrode was tied to ground through a 2 kΩ resistor and the rear electrode floated. The nozzle was grounded directly. The rear electrode spin coil was operated both in series with the arc or separately excited. The forward electrode spin coil was always in series with the arc. The power pins for the forward coil can be seen in Fig. 1.

The rear inspection port was redesigned to allow viewing the arc using high speed motion pictures. Details of the viewing window and the camera set-up are contained in Section 2.3.

11—3223
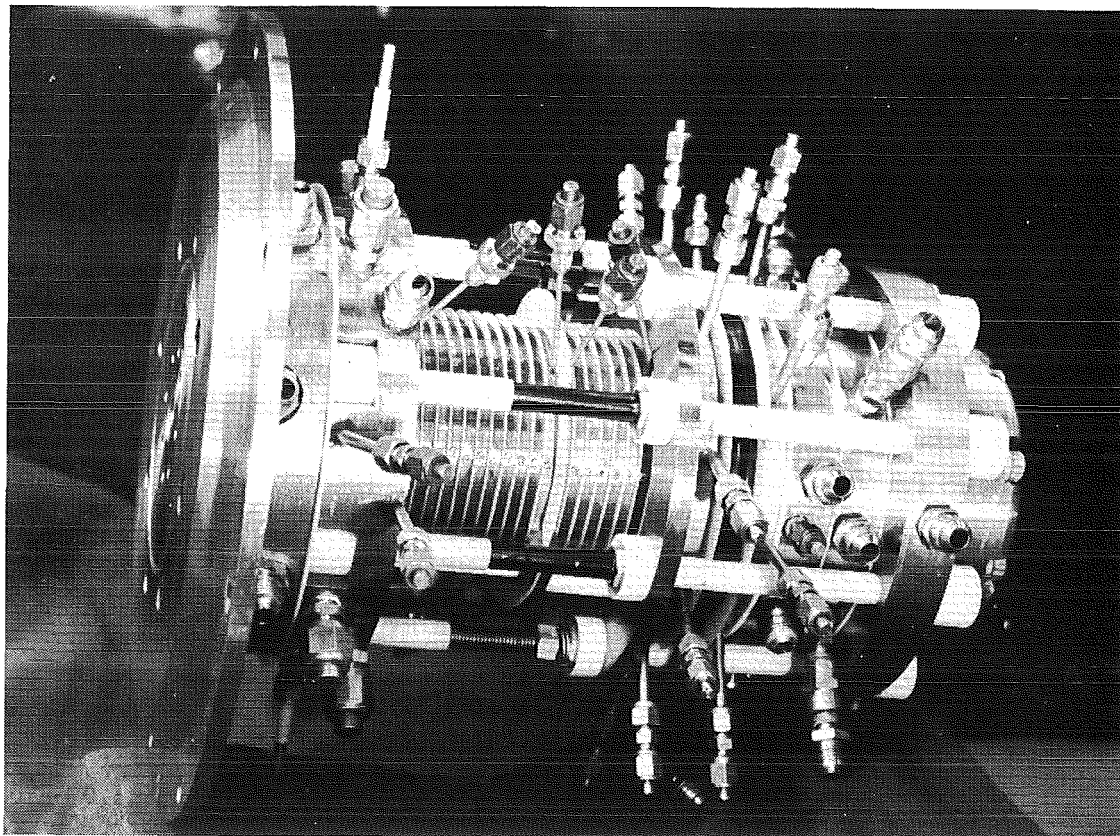
Figure 2. HIPERARC assembly

2.2 TEST FACILITY

This program was conducted in the MDAC LCAT facility. The control room and test stand of the LCAT is shown in Fig. 3. The arc heater can be seen through the projectile proof window from the control console. The exhaust of the arc heater inside the test cabin was viewed on a color television monitor. The test cabin was evacuated using a steam ejector vacuum system.

All of the instrumentation outputs were routed to the LCAT control room where they were recorded on magnetic tape or on a recording oscillograph. The normal oscillograph paper speed was 20 in./s yielding a 50 in. record for a 2.5 s test. All component potentials, arc current, arc pressures and interlock information were recorded on the oscillograph. All outputs except the component potentials were recorded on magnetic tape for later reduction by computer to engineering units. The resultant data were computer tabulated and printed out in a special format.

11—3224
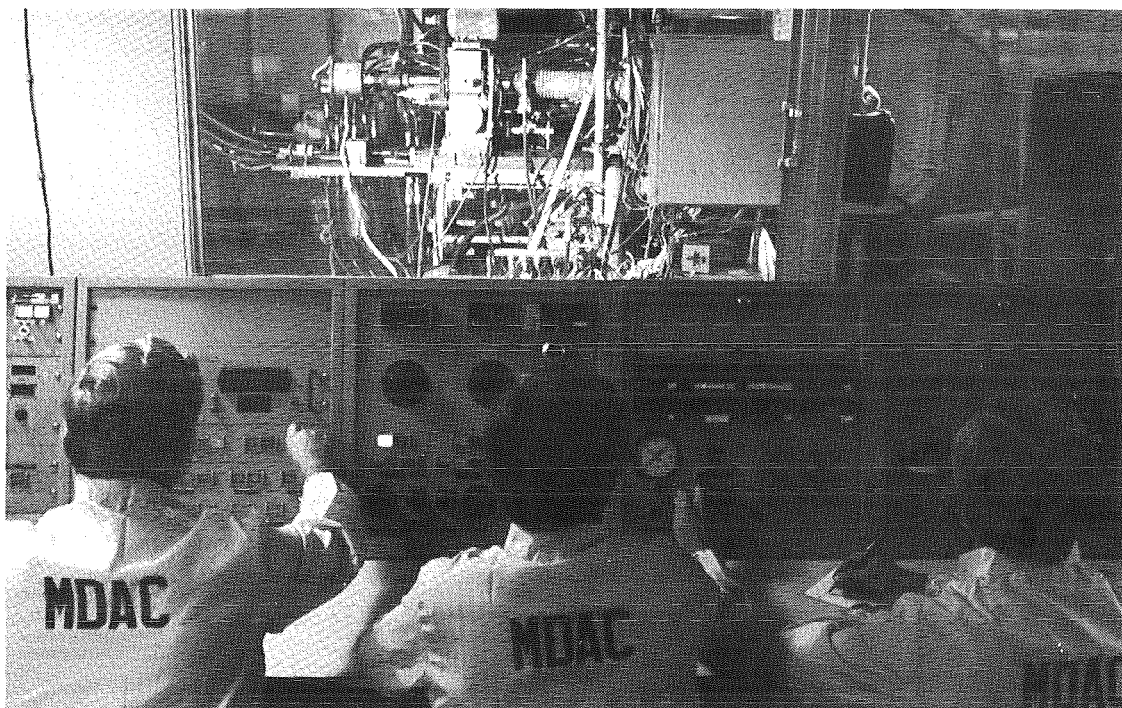
Figure 3. The MDAC LCAT arc heater facility

Modifications to the LCAT controls were made to include:

° Camera initiation prior to arcing,

° Arc voltage interlock upon intersegment arcing,

° Rapid arc current ramp,

° Simulated start to pre-set air flow, and

° Local dome loaded regulator controls.

The standard HIPERARC testing procedure was used in these experiments. Preliminary checks consisted of the following sequence:

° Bench test of HIPERARC to 200 psig gas pressure.

° Water flow check for leaks and proper flow rate with HIPERARC installed in LCAT.

° Set interlocks.

° Pressure test of installed HIPERARC to 25% higher than anticipated running pressure.

° Measure arc heater gas flow rate and distribution using a nozzle orifice (mounted downstream of the HIPERARC nozzle) that simulates hot flow pressures in the heater.

° Adjust ramp rate.

° Voltage test each arc heater component to ground to ensure individual isolation.

Immediately prior to a test the following tasks were conducted:

° Directed the boiler operator to supply steam to the steam ejector vacuum system.

° Secured vacuum system.

° Loaded cameras with film.

° Focused television camera on the nozzle exit and placed tape recorder on stand-by.

° Satisfied subsystem interlocks and secured the LCAT test area.

° Activated water pumps and recorded flow rates.

° Calibrated data acquisition tape and placed on stand-by.

° Demagnetized the saturable reactor cores in the power supplies.

° Adjusted potentiometer for desired arc current.

° Loaded gas flow regulator to desired flowmeter pressure.

° Checked ramp time and total time; then re-set on-off gas valve and test timer.

° Adjusted interlock voltage for 500 V less than anticipated arc voltage.

° Set voltage interlock activation time.

° Closed the fused disconnects on each power unit required.

The arc heater was then ready to start. The following sequence occurred during a test:

° Turned on data recording equipment (data tape, oscillograph, and television).

° Turned on camera stand-by circuit.

° Activated power supplies which also triggered the camera start.

° Initiated the arc via vacuum break-down inside the heater. As arc current flowed, the gas flow valve opened and gas flow ramped to the desired flow rate in the pre-set time.

° Monitored television screen and observed the arc heater exhaust visually.

° Secured or placed in stand-by all systems for the next test.

The standard ramp time was 1.5 s and the standard test duration using uncooled constrictor segments was 1.5-2.5 s.

The LCAT subsystems required for HIPERARC operation were the air, water and power supplies. The high pressure air supply consists of 15 tanks each with 19.4 ft^3 volume rated at 6420 psig. This supply will allow testing for up to 9.4 min at 250 atm arc pressure using a 0.375 in. diameter nozzle throat. Two multi-stage centrifugal water pumps which combined are capable of 700 gpm at 1200 psi plus 500 gpm at 600 psi are available. Only one pump was used for these tests and the inlet water pressure to HIPERARC was 580 psig. The primary arc power supply in LCAT has four modules with a combined open circuit voltage of up to 20 kV and a maximum power of 10 MW for 6 minutes. Normally only one module of that supply was used for these tests. Thus the open circuit voltage was 5 kV. Some tests used two modules in series for 10 kV. The modules are basically silicon diode rectifiers with saturable reactor current control. Each module has an internal inductance of 8 mH. All four units were linked in series to gain this circuit inductance even though only one or two modules were activated.

13

2.3 MOTION PICTURE CAMERAS

Arc motion was photographed through a quartz window at the rear of the heater and for some tests through the nozzle throat using a mirror in the heater exhaust.

The rear camera was a Hycam Model K20S4E. This camera can expose 400 ft of film at speeds from 20 to 11,000 frames/second (fps). It is a 16 mm format rotating prism camera. All motion pictures taken in this program used 16 mm commercial film (Eastman Kodak Ektachrome 7252 or 2256). A timing light in the camera provided time references on the side of the film at a frequency of 100 Hz.

Framing rates for all tests were nominally either 5000 fps or 10,000 fps. The actual frame rates and frame counts varied slightly due to different response to arc initiation. Figure 4 shows a typical frame rate vs frame count for the camera at a nominal 5000 fps setting. This characteristic was fairly repeatable. The frame rate and frame count as a function of time for the 10,000 fps setting is shown in Fig. 5.

The shutter ratio for these tests was 1/10. Ample light from the arc events allowed this setting. The high arc intensity demanded high aperture settings and neutral density filters.

The optical arrangement included a 105 mm (f/2.8) Takumar lens with a Curvator lens attachment. The 105-Curvator attachment yielded an effective focal length of 35 mm while providing extended depth of field. The wide band of acceptable field was necessary to observe the arc in the constrictor and beyond. The Spireton Curvator auxiliary lens attachment provided a wide range of effects from true circular "fish eye" format to full frame coverage with only moderate curvature.

11-3210
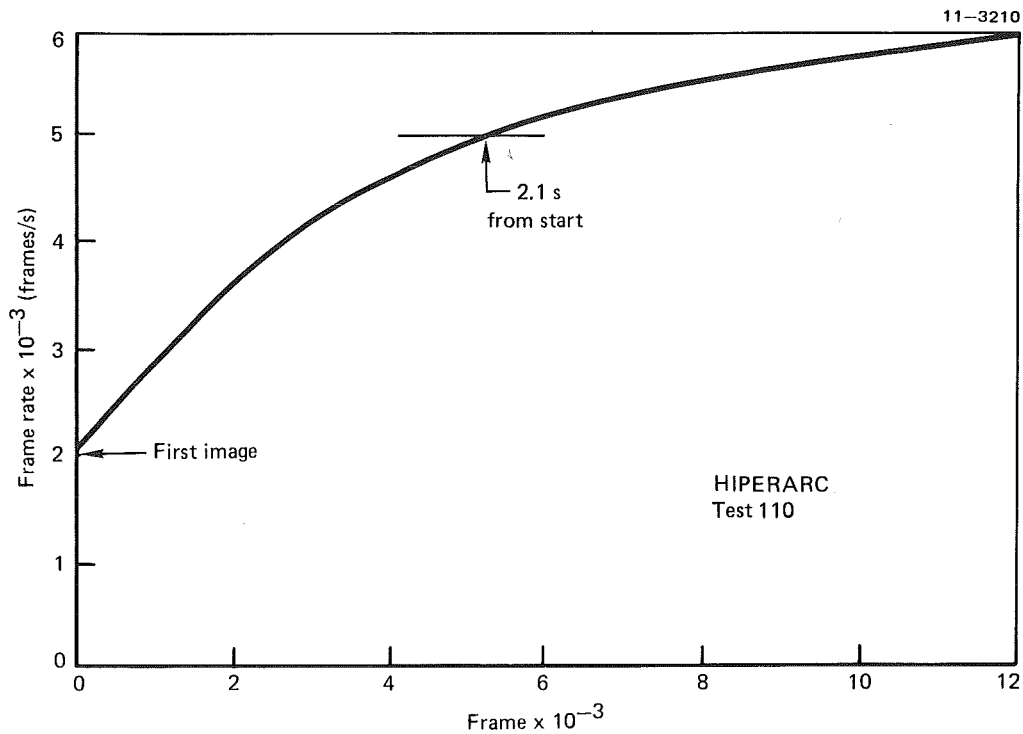
Figure 4 Hycam camera frame rate (nominal 5000 frames/s)

11-3209
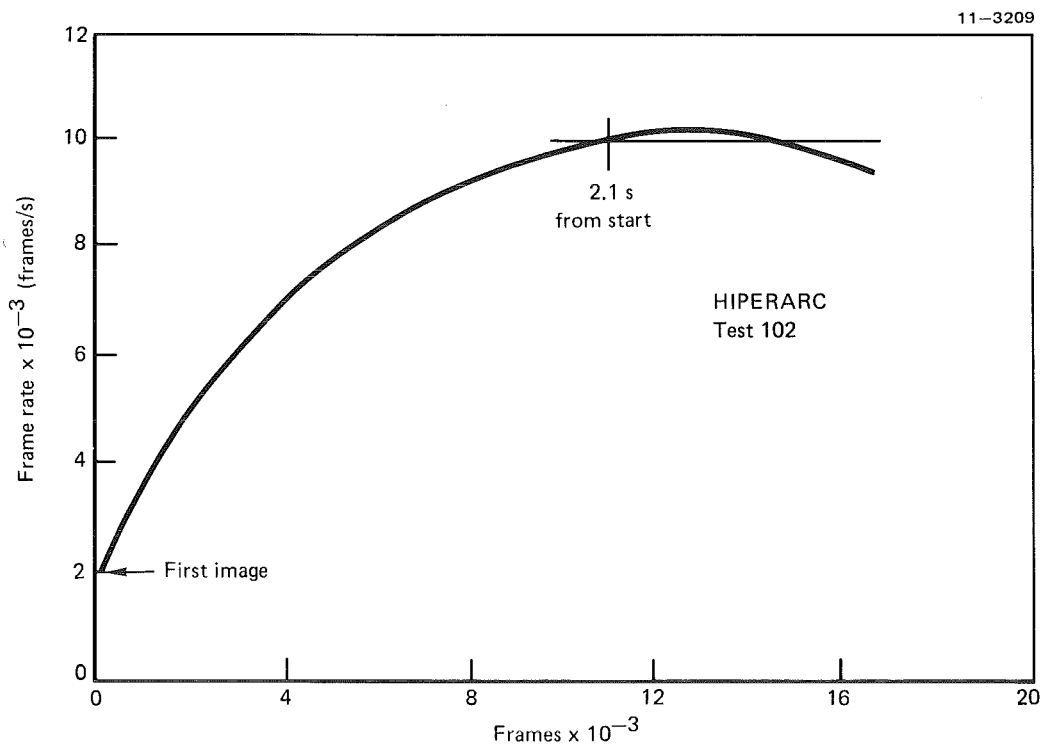
Figure 5 Hycam camera frame rate (nominal 10,000 frames/s)

The distance from the lens to the rear electrode mid-plane was 24.6 in. for most of the tests. The camera was sighted through a quartz window designed specifically for these tests. Figure 6 shows the window design. Provisions for measuring the arc chamber pressure and for bathing the inside window surface with cold air were incorporated in the window holder. The gas flow rate varied from 1 to 2% of the total gas flow rate with the tangential injection augmenting the primary swirl.

11—3208

Retainer plate

Arc pressure tap

Gas injector ring

Quartz viewing window

Gas injector

0 _____ 1
Scale — in.
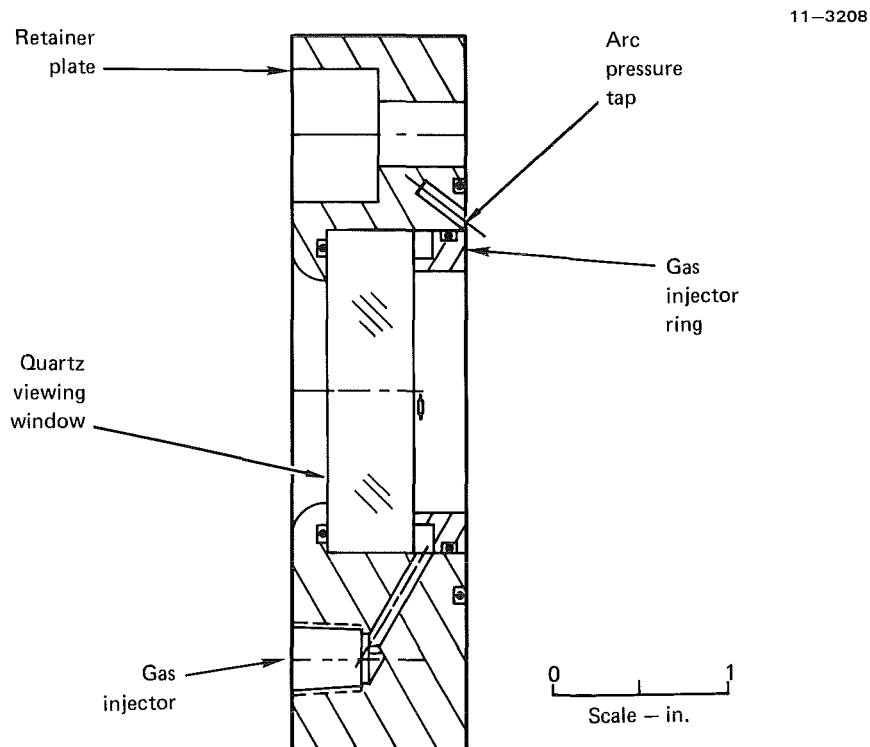
Figure 6 Arc viewing window

3.0 ARC HEATER CONTROL EXPERIMENTS

The objective of this work was to conduct experiments aimed at improving methods of controlling a high pressure, high current arc in a high performance constricted arc heater.

The approach was to vary the primary parameters that control the arc stability, location and characteristics in a high performance arc (HIPERARC) heater and to photograph the effects of those variations using high speed cameras. The motion picture data were then correlated with other recorded data to evaluate the effects of the control parameter variations.

Table 1 summarizes the arc control experiments conducted with HIPERARC. All parameter ranges exceeded the initial goals and the total number of tests was 2.5 times the expected number at the outset of the program. In addition, tests conducted with the larger nozzle prior to this program are included in the analysis for completeness.

Table 1 Summary of arc control experiments

11—3217

Nozzle throat diam. (in.)	0.530	0.375
Total tests conducted	11*	39
Control parameter variation	Range **	
Arc current (A)	0—830	0—720
Arc pressure (atm)	0—50	0—50
Air flow rate (lb/s)	0—1	0—0.5
Starting ramp rate (s)	1—2	1—2
Segment resistance (MΩ)	0.15—20	0.15—20
Spin coil current (A)	300—830	300—720
Gas injection distributions	4	5
Constrictor length (in.)	8.3—11.6	8.3—11.6
Arc polarity	S, O	S, O
Camera frame rate (kf/s)	5, 10	5, 10

*Does not include earlier tests

**Does include earlier tests.

Table 2 is a summary of the six arc heater assemblies tested to acquire
the data in this report. The first two assemblies were tested previously.[5]
The final four assemblies were tested during this program. Each assembly
required a complete removal of the arc heater from the test stand and
included a thorough analysis of the arc tracks and damage prior to modifica-
tions and reinstallation. Variations in the gas flow distribution were made
for a given assembly by inserting control orifices in the various gas lines.

Table 2   Experimental arc heater assemblies

11—3218

Assembly	Nozzle	L/D	Test Nos.	Comments
1.	0.530	9	69—84	Pre-contract water-cooled energy balance data[5]
2.	0.530	13	87—104	Pre-contract uncooled with high speed films[5]
3.	0.530	13	105—115	New quartz window Conducted variations
4.	0.375	13	116—122	Intersegment arcing destroyed hardware
5.	0.375	13	123—136	Improved circulation Intersegment arcing
6.	0.375	9	137—154	Improved circulation Reduced field coil strength Conducted variations

3.1 CONTROL PARAMETER VARIATIONS

The experimental techniques used to vary the arc control parameters
are described below along with their limitations. The effects of these
variations on arc control are discussed in Section 4.

3.1.1 Arc Current Variations

The arc current was controlled through adjustments in the saturable
reactor current in the arc heater power supply. Two control potentiometers
were used. The first was pre-set at a low level (25% of full saturation)
to limit the initial current spike on arc breakdown. The second was pre-set
between 73 and 87% to establish the final arc current level. The second

setting was adjusted for the open circuit voltage (number of power supply modules) and the arc voltage demand (air flow rate). In general the desired arc current could be pre-set within $\pm$ 50 A unless arc instabilities occurred.

In addition to the variations in final arc current, considerable data were acquired during start-up and shut-down or blow-out. Thus, although the final current variation was limited to the 300 to 830 A range, considerable data were acquired at lower (and sometimes higher) levels for brief periods.

3.1.2 Arc Pressure and Air Flow Rate Variations

The arc pressure was controlled through variations in the air flow rate and nozzle throat area. A factor of two change in the nozzle area allowed comparisons at the same pressure with approximately twice the air flow rate. The air flow rate was pre-set using a large dome loaded regulator. The cold flow arc chamber pressure was used as a guide in setting the flow rate such that the desired final hot flow pressure was reached. The arc pressure was monitored at the edge of the quartz viewing window in the rear of the heater (Fig. 6) using a standard transducer. The air flow rate was monitored using a subsonic Venturi.

3.1.3 Starting Ramp Rate

The ramp time in which the air flow was increased from near zero at arc breakdown to its steady value was varied from 1 to 2 s using a throttle valve in the load line of a local regulator. The regulator was near the gas injector manifold. The gas flow rate into the heater was limited on start to a value that maintained a pressure inside the heater at 10 Torr or less. Arc ignition triggered the regulator load solenoid valve and the pre-set load throttle valve controlled the ramp rate. The ramp time from zero flow to steady-state was repeatable within 0.1 s. The hot flow ramp required slightly longer times than the cold ramp due to power stabilization requirements.

3.1.4 Segment to Ground Resistance Variations

Since the converger and constrictor segments in these tests were uncooled, excellent electrical isolation was achieved. The natural resistance to ground on all segments was greater than 20 MΩ. Water-cooled segments

have a grounding resistance that varies with the length and number of coolant hoses as well as the conductivity of the coolant. Previous tests with HIPERARC indicated this resistance to be the order of 150 kΩ. These two resistance levels were tested at near identical conditions to determine if the normal coolant hose resistance was a factor in such instabilities as inter-segment arcing. Wire wound resistors were connected between each segment and ground for the low resistance tests.

3.1.5 Spin Coil Current Variations

The 12-turn rear electrode spin coil is electrically isolated from the electrode housing (Fig. 1). This feature allows separate or series excitation of the coil. For separate excitation a 60 kW saturable reactor power supply was connected to the coil with separate console controls. Spin coil current levels of 400 and 300 A were tested. The coil was excited prior to arc ignition resulting in a stronger initial field but a weaker on-condition field near the rear electrode. A serious problem with separate excitation resulted from arc blow-out. The coil was essentially grounded through its water cooling connections (150 kΩ) and thus high voltage transients on blow-out would result in arc-over to the coil and subsequent damage to the coil power supply. The coil power supply was not isolated against voltages above 600 V. A spark gap set for 10 kV was installed across the arc power supply to dissipate arc transients. This relieved the transients on several tests but the final test (154) encountered arcing to the coil in spite of the arc gap. Improved isolation of the coil will be necessary for future testing.

3.1.6 Gas Injection Distribution Variations

Table 3 summarizes the air flow distributions tested. Normally the distribution was dictated by the area of the injectors at a given location since the injection velocity was low subsonic at all stations. Modifications to the distribution were made using small in-line orifices at the arc heater. Changes could be made easily without disassembly of the heater.

Table 3 Air flow distributions (%)

Tests	d^* (in.)	Rear window	Rear retard	Rear electrode	Converger	Constrictor	Front slot	Front retard
69—84	0.530	0	7.8	53.1	7.6	26.7	0	4.7
87—104	0.530	0	9.5	36.1	9.1	32.4	8.2	4.8
105—107	0.530	1.2	10.3	39.2	9.8	35.1	3.0	1.5
108—109	0.530	1.1	8.3	33.3	8.3	35.7	9.0	5.3
110	0.530	1.0	6.7	26.7	6.7	42.8	10.9	6.3
111—114	0.530	1.2	10.3	39.2	9.8	35.1	3.0	1.5
115	0.530	1.2	9.3	35.9	8.9	32.2	8.0	4.6
116—118	0.375	1.2	10.3	39.2	9.8	35.1	3.0	1.5
119	0.375	1.3	4.4	41.7	10.5	37.3	3.2	1.6
120	0.375	1.3	3.0	42.0	10.6	38.0	3.3	1.7
121	0.375	1.7	3.9	55.6	13.9	18.6	4.2	2.1
122	0.375	1.9	4.0	61.4	15.4	10.0	4.7	2.3
123—127	0.375	1.2	3.8	46.0	10.0	34.0	5.4	1.2
128—130	0.375	1.2	4.0	45.0	9.7	33.2	5.4	1.2
132—133	0.375	1.1	5.6	44.6	9.5	32.5	5.6	1.2
134—136	0.375	1.1	9.5	42.8	9.1	31.2	5.4	1.1
137—154	0.375	1.3	11.2	50.6	10.7	18.5	6.3	1.3
Flow ranges (%)								
69—115	0.530	0—1.3	6.7—10.3	26.7—53.1	6.7—9.1	26.7—42.8	0—10.9	1.5—6.3
116—154	0.375	1.1—1.9	2.8—11.2	39.2—61.4	9.1—15.4	10.0—38.0	3.0—6.3	1.1—2.3

Tests	Primary	Constrictor	Front slot	Front retard
69—154	40.0—82.7	10.0—42.8	0—10.9	1.1—6.3

A change in the constrictor length changed the constrictor injection area and modified the flow distribution. For example, the last test series had only 18.5% of the flow through the shortened constrictor.

Calibrations of the individual station areas were conducted under sonic flow conditions, i.e., injector pressure more than twice the arc chamber pressure using cold flow. The effective areas were all less than the measured physical areas but the distributions were not affected significantly.

3.1.7 Constrictor Length Variations

The changes in constrictor length for continued small nozzle testing were in lieu of the originally planned changes in rear electrode geometry. Removal of one module of twelve constrictor segments required complete disassembly of the heater and substitution of shorter main assembly bolts. In addition the camera was moved to maintain the same view. The reduction in constrictor length in this program resulted in an L/D reduction from 13 to 9. This same reduction was made previously for large nozzle tests.[5] These data are included for comparisons herein.

3.1.8 Arc Polarity Variations

The HIPERARC heater is normally operated with the rear electrode positive (anode) and the forward electrode negative (cathode) with the nozzle grounded. The forward electrode is tied to ground through a 2 kΩ resistor. Reversing the polarity required reversal of the power leads to the arc heater and reversal of all component potential leads (15 channels). The arc heater power supply did not require any modifications. The interlock based on arc voltage was also reversed. For those tests where a separately excited spin coil was used with reversed arc polarity, the coil connections were also reversed to maintain an augmenting field.

3.2 EXPERIMENTAL DATA

The experimental data acquired during this program are in three formats: (1) the motion picture data are contained on 400 foot reels of 16 mm film; (2) the 15 component potentials, arc current, injection pressure, arc pressure, test time and interlock signals are contained on oscillograph traces, and (3) the magnetic tape data have been converted to engineering units and computer tabulated. The arc events and timing lights on the films allow correlation of these data with the oscillograph recordings.

The brevity of the tests (< 3 s) reduced the accuracy of some of the magnetic tape data since most of the sampling was done at 100 channels/s. Later tests (142-154) were sampled at twice this rate after improving the instrumentation ground.

3.2.1 Motion Picture Data

Table 4 summarizes the 300,602 frames of motion picture data acquired using HIPERARC. The films of each test have been viewed using a Lafayette 16 mm film analyzer which allows stop action and multiple speed projection. Significant events from the films were correlated with the oscillograph recordings.

Table 5 summarizes the tests selected for detailed analysis of the effects of arc control parameters. The range of the parameters is shown for each nozzle tested. The ranges were generally established to yield comparative data without undue sacrifice of hardware caused by gross instabilities.

In addition to the parameter variations from one test to another, considerable comparative data were gleaned from variations during a single test. The motion picture data were acquired at rates up to 10,800 fps and thus provided several frames of an event that occurred in a very short time period. For example, a typical arc spiral and then arc shunt would occur in 0.02 s which would be recorded on 100 to 200 frames of data. That same event would extend over 0.4 in. on the oscillograph recording making correlation relatively easy.

Some of the observed arc phenomena from these experiments are listed in Table 6. Typical events are depicted in Fig. 7 where visual comparisons can be made for the different variations of control parameters. These show the wide variety of arc instabilities encountered. A full appreciation of the events and characteristics can only come from viewing the films and monitoring the oscillograph recordings for each phenomenon.

Section 4 of this report compiles the analyses conducted on these motion picture data. Additional analysis would undoubtedly yield more insight into the effects of control variables on arc behavior.

Table 4 Motion picture data summary

Test no.	Final frame rate (fps)	Total frames	Final arc pressure (atm)	Final arc current (A)	Arc control parameter variation
Nozzle throat diam. 0.530, L/D = 13					
87	6700	4850	20	240–450	Arc current
88	7500	4900	20	430–510	Arc current
89	7600	4932	25	400–500	Arc pressure
90	7300	4800	25	400–500	Repeat
94	9700	15423	25	650–750	Arc current
99	10800	15486	32	600–700	Arc pressure
106*	4200	3145	12	270–420	Arc current
107	5900	11743	24	650–700	Arc current
109*	5200	8314	23	540–700	Flow distribution
110	5920	11790	25	740	Flow distribution
112*	4700	4203	16	390–450	Ground resistance
114	4920	4860	17	450	Opposite polarity
115	4800	4270	16	450	Opposite polarity
Nozzle throat diam. 0.375, L/D = 13					
117	4980	5862	22	450–530	Air flow rate
118*	5210	6323	23	510–780	Arc current
119	5320	6703	24	600–650	Flow distribution
120*	5860	12023	29	650–720	Arc pressure
121	——	5062	19	460–540	Constrictor flow
122	4590	4070	21	450–540	Constrictor flow
124*	4470	3928	22	600	Injection radius
125	3660	2032	15	270	Short ramp
127	5000	5902	29	600–650	Spin coil current
130	4540	4185	24	500	Arc pressure
133	3240	3560	27	450	Arc pressure
134	5190	5692	30	500–600	Arc pressure
Nozzle throat diam. 0.375, L/D = 9					
138	4740	4325	21	600	Constrictor length
139	5480	8238	29	600–800	Air flow rate
140	4810	5235	21	480–550	Arc current
141	5500	8326	26	500–600	Arc current
142	5850	8743	24	540–600	Spin coil current
143	4920	5313	22	600	Spin coil current
144	5580	8657	25	510	Spin coil current
145	9560	12582	26	500–540	Frame rate
146	9870	11482	38	500	Arc pressure
147	10170	10275	33	500	Arc pressure
148	4270	1156	——	——	Water leak
149	9810	13357	26	550	Arc pressure
150	10050	11728	26	550	Opposite polarity
151	9460	8905	25	500	Ground resistance
152	9650	13680	25	500	Ground resistance
153	7760	4542	36	550–600	Arc pressure

Total frames 300,602   *Additional films of front electrode through nozzle.

Table 5 Arc control variation comparisons

11—3226

Parameter	Comparison tests	Nozzle d* (in.)	Variation range
Air flow rate	99, 127, 120	.53—.375	0.46 → 0.24 lb/s
Arc pressure	107, 99	0.530	25—32 atm
	149, 146	0.375	25—38 atm
Gas flow distribution %P/%S	107, 109, 110	0.530	60/40, 50/50, 40/60
	120, 121, 122	0.375	56/44, 75/25, 82/18
	130, 133, 134	0.375	Rear retard 5.6/9.5
Ramp rate	130, 125	0.375	1.5 → 1.0 s
	149, 153	0.375	1.5 → 2.0 s
Arc current	107, 109	0.530	300 → 750A @ 24 atm
	133	0.375	400 → 600A @ 25 atm
	153	0.375	375 → 600A @ 37 atm
Spincoil current	130, 127	0.375	Separate v.s series
	141, 142, 144	0.375	Series → sep. 400A → sep. 300A
Arc polarity	107, 114	0.530	Anode → cathode
	149, 150	0.375	Anode → cathode
Seg-gr resistance	107, 112	0.530	> 20 MΩ → 150 kΩ
	149, 152	0.375	> 20 MΩ → 150 kΩ
Constrictor length			
Series coil	99,	0.530	L/D 13
Series coil	130, 139	0.375	L/D 13 → 9
Separate coil	127, 142	0.375	L/D 13 → 9

Table 6 Arc events and characteristics filmed

11—3219

1. Arc breakdown phenomena
2. Arc attachment on electrodes and rotation
3. Arc stabilization
4. Arc spirals in converger
5. Arc kinking along column
6. Intersegment arc over (partial and complete)
7. Arc column shunting to wall
8. Arc column shunting within core
9. Arc growth with current
10. Arc size reduction with pressure
11. Arc sheeting at high pressure
12. Shroud gas radiation
13. Arc blow-through nozzle
14. Arc blow-out and current decay
15. Effects of water leak on arc behavior

Large nozzle
$d^* = 0.530$ in.

Small nozzle
$d^* = 0.375$ in.

11—3241

Camera
view

Arc
breakdown

Camera
view

Arc
breakdown

Low   Arc pressure   High

Low   Arc pressure   High

Low   Arc current   High

Low   Arc current   High

Low   Air flow rate   High

Low   Air flow rate   High

Figure 7. Typical filmed arc events

Large nozzle
d* = 0.530 in.

Small nozzle
d* = 0.375 in.

11—3242

Short   Long
Starting ramp time

Short   Long
Starting ramp time

$R_g = 150k\Omega$ $R_g > 20 M\Omega$
Segment grounding resistance

$R_g = 150k\Omega$ $R_g > 20M\Omega$
Segment grounding resistance

Low   High
Spin coil current

Low   High
Spin coil current

Not
available

Short   Long
Constrictor length

Short   Long
Constrictor length

Figure 7 Typical filmed arc events (continued)

27

Large nozzle
d* = 0.530 in.

Small nozzle
d* = 0.375 in.

11—3243

| 60/40 | 40/60 | 83/17 | 60/40 |
| Gas flow distribution (primary/secondary) | | Gas flow distribution (primary/secondary) | |

| Standard | Reverse | Standard | Reverse |
| Arc polarity | | Arc polarity | |

| Converger | Constrictor | Massive |
| Intersegment arc over | | |

| Blow-through | Roll-over | Kinking | Sheeting |

Figure 7 Typical filmed arc events (continued)

28

3.2.2 Oscillograph Recorded Data

A Honeywell Model 1612 Visicorder oscillograph was used to record 15 component potentials, arc current, arc pressure, injector pressure and interlock information. A complete record of each test was acquired at 20 in./s paper speed. Thus a 2.5 s test yielded a 50 in. long record. Timing lines were recorded each 0.1 s for correlation to the filmed data.

Figure 8 shows a typical test recording. The component potentials (except the rear electrode) and the photo cell output were located on one side of the trace deflecting positively toward the center. The remaining information was located on the opposite side also deflecting positively toward the center. The standard sensitivity for all potentials was 1000 V/in. Thus relative potentials could be easily determined. The arc current sensitivity was 300 A/in. and the pressures were 26.7 atm/in.
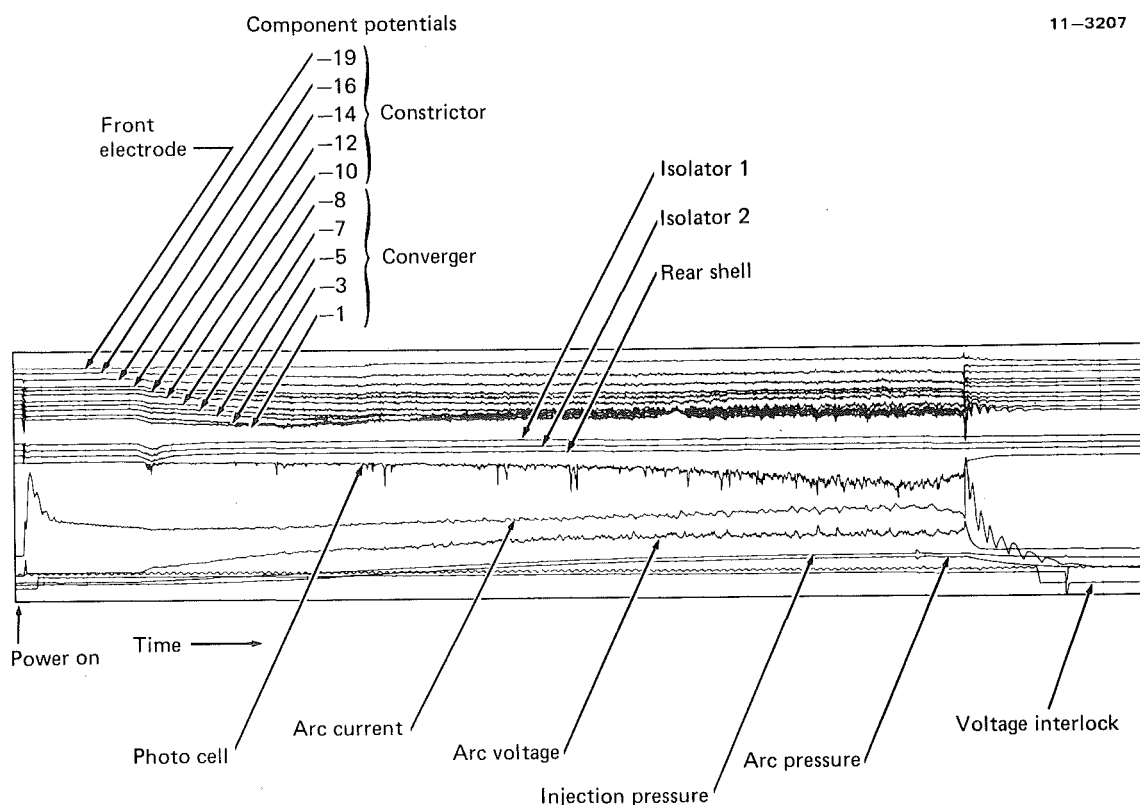

Figure 8   Typical oscillograph recorded HIPERARC test

29

The history of an arc heater start is described in Section 4.1.4 and the effects of ramp time are presented there.

The occurrence of arc instabilities could be observed immediately following a test using the oscillograph recording. Correlation of these events was accomplished the following day when the developed film was available.

3.2.3 Magnetic Tape Recordings

Forty-three channels of the LCAT data acquisition system were dedicated to these tests. The initial sampling rate was 100 channels/s yielding only five data points in a 2.5 s test. Higher sampling rates caused severe noise in the data. Later in the program an improved grounding system allowed sampling at 200 channels/s yielding 10 data points in a 2.5 s test. These data were used primarily for pre- and post-test references where steady values were recorded. The on-condition arc current, voltage and pressure served as a back-up to the oscillograph.

The only primary data from the tape recordings during test were the mass flow rates. Previous tests for longer time periods indicated steady gas flow rates were reached in 2.0 s or less. The recorded mass flow rates are discussed in Section 4.1.1.

Complete records of all 43 parameters are on file at MDAC in engineering units for each test conducted. In addition, these data were compiled using a HIPERARC code and printed out in a user format. However, due to the slow sampling rate and the brevity of these tests, these calculated data are not generally steady-state values and as such are of limited use. The printed arc current, arc pressure, arc voltage, arc power, injector pressure ratio and water flow rates are accurate. The final mass flow rate on tests longer than 2.0 s and the pre- and post-test information are also accurate. The water flow rates are printed for each component prior to the arc ignition. Subsequently the power loss, computed from the differential temperature sensor and water flow rate, are printed for each component.

4.0 ARC CONTROL PARAMETER EFFECTS

The design of an arc heater is dictated by the desired effluent
characteristics, available subsystems, and the need for arc control.
Once the design is established, the arc heater experimentalist is limited
to three general areas which he can modify to control arc heater perform-
ance: (1) air flow, (2) electrical, and (3) geometric parameters. The
specific arc control parameters investigated in these experiments are
classified within these three categories in Table 7.

Table 7 Arc control variation groups

11—3215

Air flow parameters	Electrical parameters	Geometric parameters
Air flow rate Arc pressure Injection distribution Starting ramp rate	Arc current Spin coil excitation Arc polarity Segment — ground resistance	Nozzle area Constrictor length

4.1 AIR FLOW CONTROL EFFECTS

The air flow within an arc heater is critical to the performance and
stability of that heater. For a given heater geometry the arc pressure
is established by the air flow rate and the net energy imparted to the
gas. The manner in which the air is introduced into the heater establishes
the necessary forces to counter balance the destabilizing electromagnetic
forces on the arc column. The distribution of the air flow throughout
the heater controls the arc column stability and the location of the anode
and cathode of the arc. The manner in which the air flow rate is increased
on starting determines whether a stable condition will be reached or an arc
instability will cause blowout or hardware damage. Although it is diffi-
cult to separate some of these air flow dependencies, the experiments dis-
cussed herein verify their criticality.

31

4.1.1 Arc Pressure/Air Flow Effects

The local arc pressure affects the thermophysical gas properties that control the arc voltage gradient and volumetric radiation. Since the arc pressure is nearly proportional to the air flow rate, changes in pressure also influence the convective energy exchange between the arc column and the arc constrictor. Thus the arc pressure influences both the arc energy input and losses.

The predicted performance of HIPERARC is shown in Fig. 9. These predictions were made using the SWIRL ARC code[6] with a longer constrictor than used in the present experiments. As the pressure is increased at a fixed arc current, the required air flow rate, the arc voltage, and the constrictor heat flux increase in nearly a linear manner. The core enthalpy decreases with increased pressure but not in proportion to the required increase in gas flow rate. The high pressure performance will be limited by the maximum constrictor heat flux which is the order of 12,000 Btu/ft^{2}s.
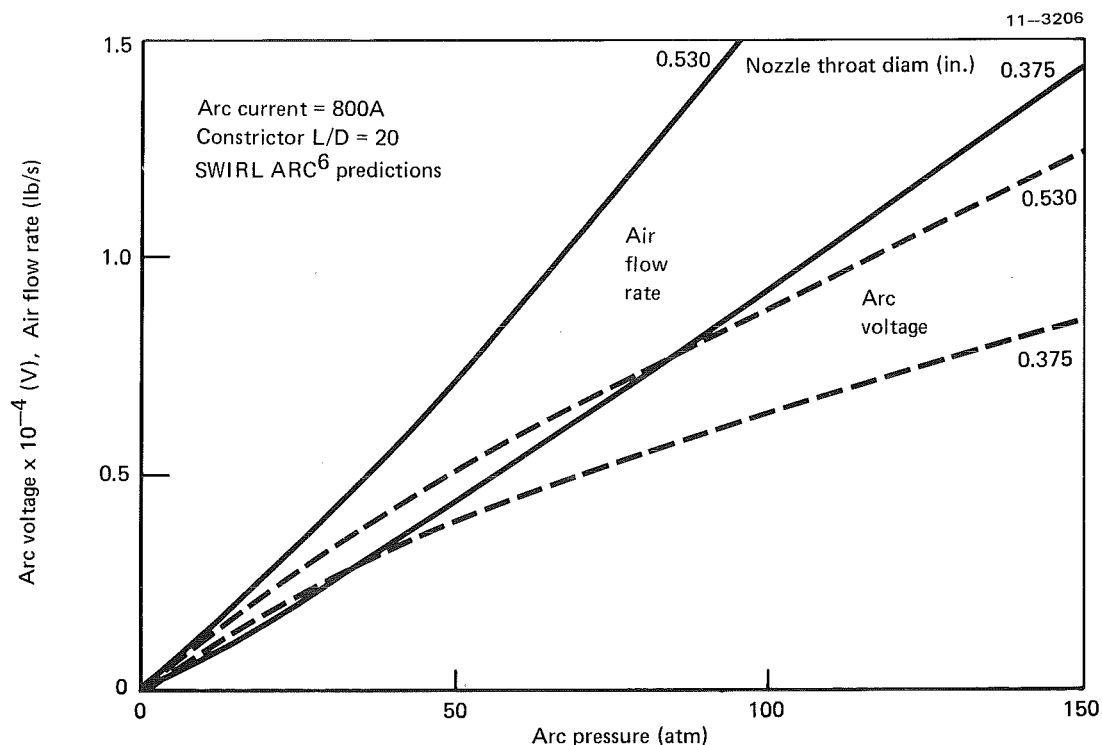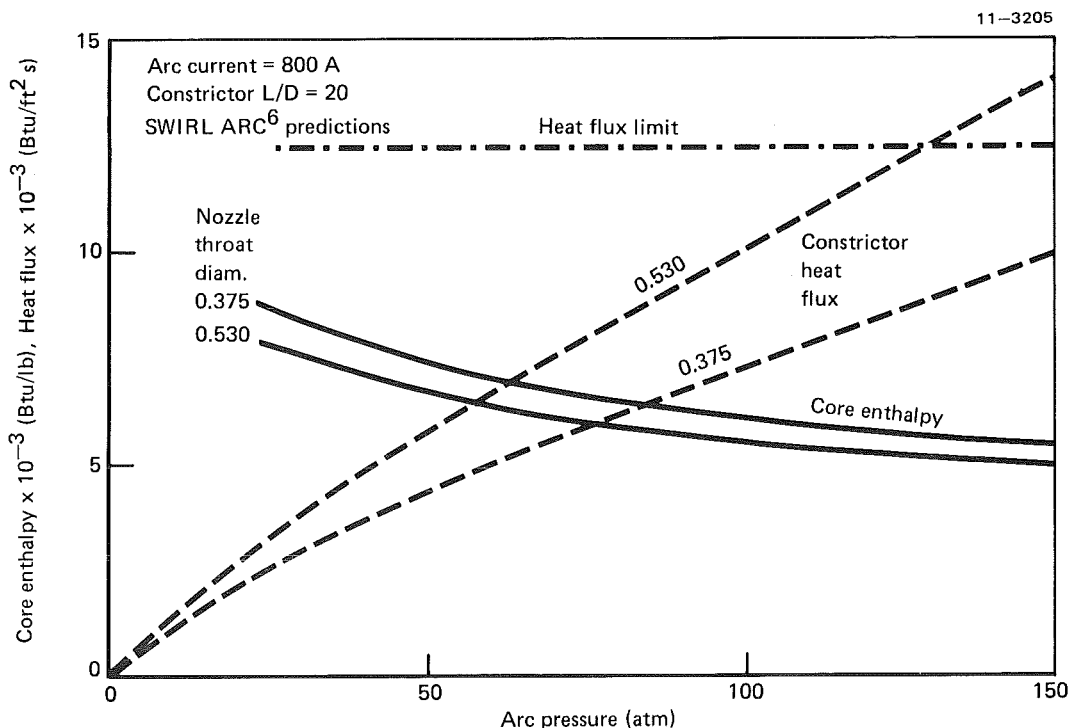

Figure 9a Predicted HIPERARC performance

Figure 9b Predicted HIPERARC pressure effects performance

The arc pressure and required air flow rates from HIPERARC experiments are shown in Fig. 10 for the 0.53 in. diameter nozzle throat and in Fig. 11 for the 0.375 in. nozzle. Data are shown for two different constrictor lengths, i.e., L/D = 9 and 13. The sonic flow equation of Winovich[7] establishes the relation between arc pressure (P_o), air flow rate ($\dot{m}$), and gas enthalpy (h_o) for a given nozzle throat diameter (d_*):

$$\dot{m} = 1.528 \, d_*^2 \, P_o \, h_o^{-0.397}. \tag{1}$$

Although the air is not uniformly heated in the short constrictors used here and there is a swirl in the flow, this relation can be used to approximate the enthalpy level of the gas emerging from the heater. Two lines of constant enthalpy are shown in Fig. 10, i.e., 1700 and 7000 Btu/lb, for comparative purposes. The experimental data indicate a smooth decrease in enthalpy with increased arc pressure (and air flow rate) which is to be expected. The data also show the enthalpy advantage of the longer constrictor. All of these data were acquired in tests of sufficient length to reach steady-state.

33

11-3204
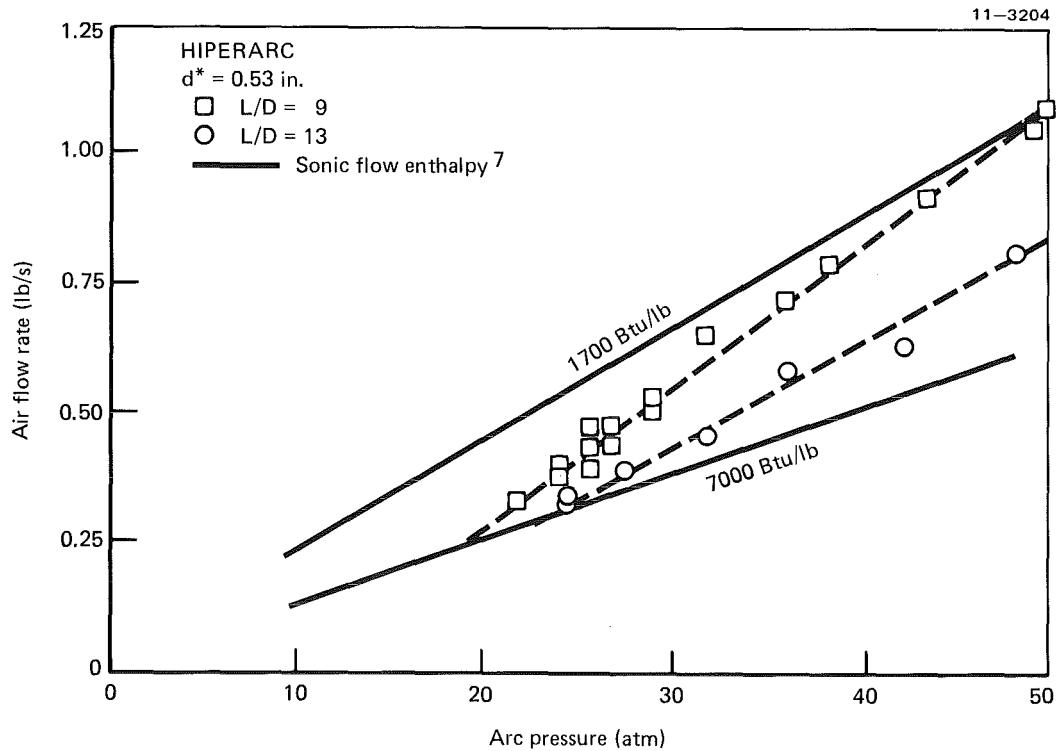
Figure 10 HIPERARC air flow rates (d* = 0.530)

11-3228
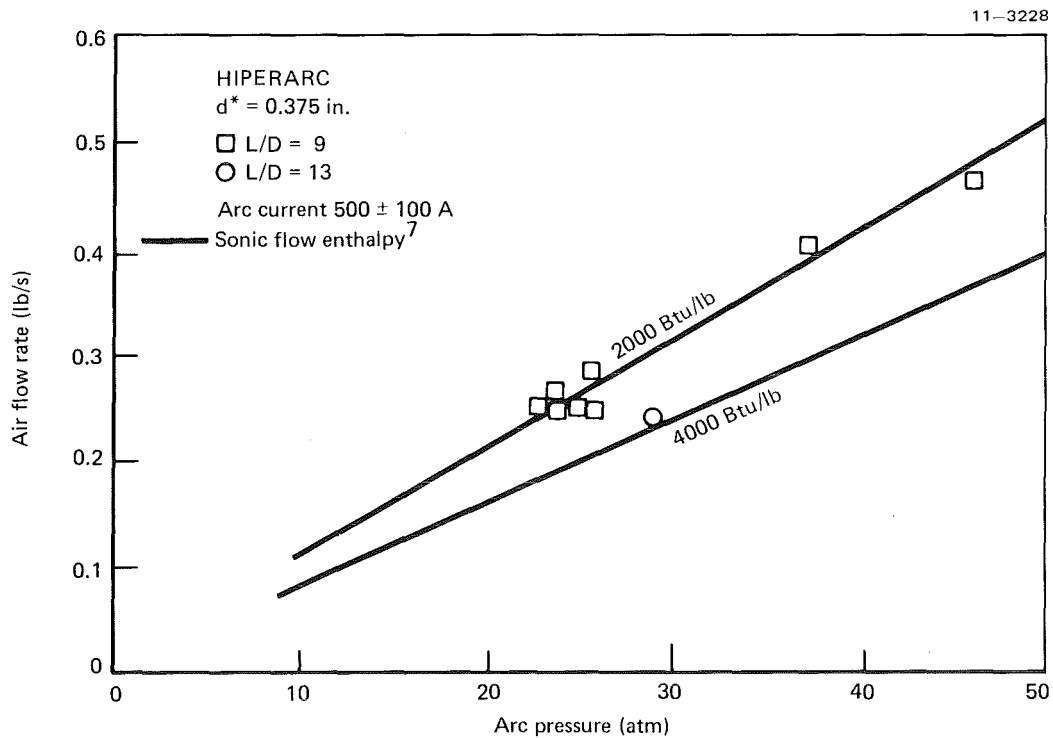
Figure 11 HIPERARC air flow rates (d* = 0.375)

Reduction of the nozzle throat area by a factor of two results in a comparable reduction in the required mass flow rate for a given pressure. The required air flow rates for the 0.375 in. diameter nozzle shown in Fig. 11 are slightly less than half those for the 0.530 in. diameter nozzle shown in Fig. 10 for the same constrictor length. The smaller throat also yields slightly higher gas enthalpies (2000 Btu/lb) at the higher pressures.

The air flow requirements, injector pressure and arc pressure are shown in Figs. 12 and 13 for typical 1.5 s ramps to 25 and 29 atm final arc pressures. The mass flow rate is ramped by a dome loaded regulator near the arc heater. It reaches a peak value before the gas inside the heater reaches its final enthalpy. As the arc current and arc voltage reach their final values, the arc pressure increases beyond cold flow levels creating a back pressure on the flow system and a reduction in the mass flow required. When the arc terminates, the arc pressure decays rapidly and the mass flow rate increases to the full cold flow value. The final cold flow mass flow rate is slightly less than the peak value due to a decrease in the Venturi pressure level, i.e., supply pressure. The accurate steady-state hot gas flow requirement is normally achieved in the order of 2 s for a ramp time of 1.5 s. Figure 14 shows the mass flow characteristic for a slower ramp (2 s) to a higher pressure (50 atm). The air flow rate reached a peak in 1 s, then remained constant as the arc and injector pressures increased to their peak levels. Following arc extinction the mass flow increased to the cold flow level.

Table 8 compiles the mass flow requirements of HIPERARC for two nozzle sizes and two constrictor lengths. These data are from those tests that were of sufficient length to establish a steady flow rate.

The measured total arc voltages in HIPERARC are shown in Fig. 15 for two nozzle sizes and two constrictor lengths. The arc voltage is a function of the arc pressure, air flow rate, arc length, and, to a lesser degree, arc current as shown in the relation:

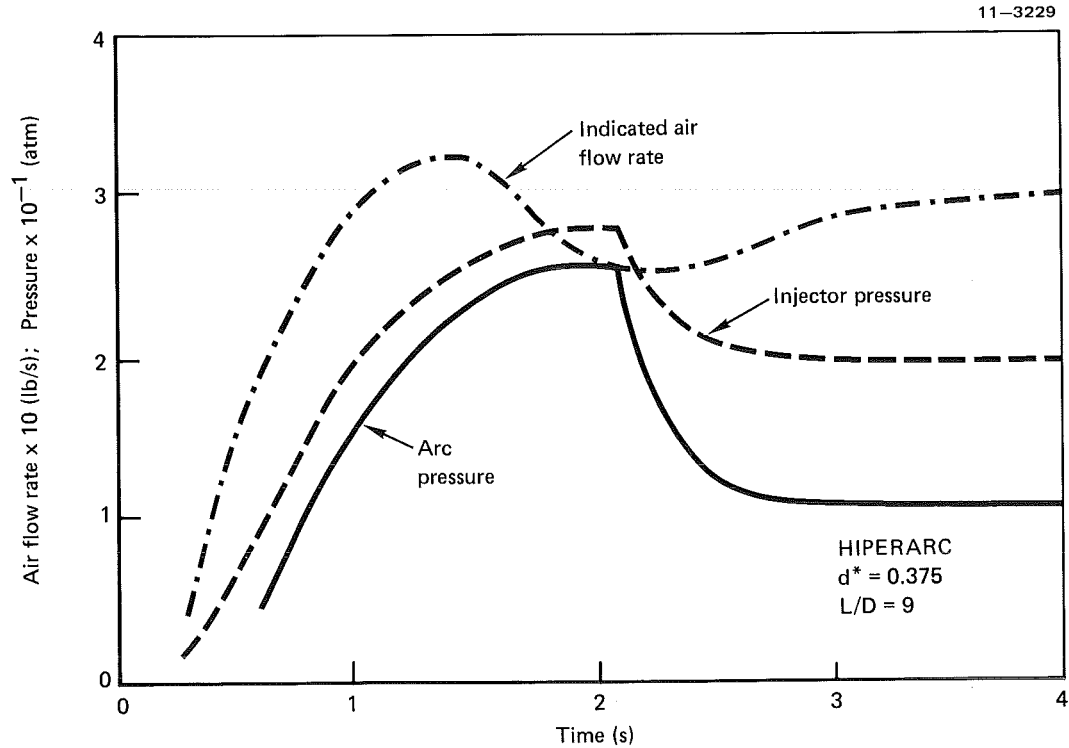$$V = C \ (L/D)^{0.75} \ (\dot{m})^{0.4} \ (P_o)^{0.165}. \tag{2}$$

11—3229

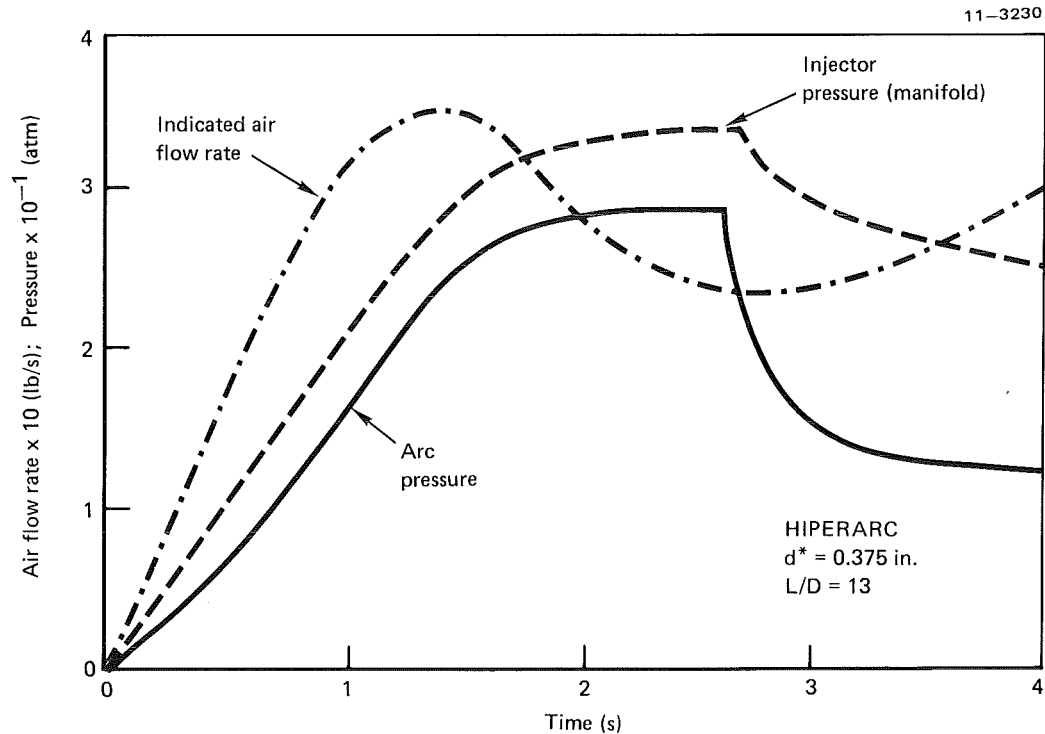Figure 12 Mass flow indicated — short ramp to 25 atm

11—3230

Figure 13 Mass flow indicated — short ramp to 29 atm
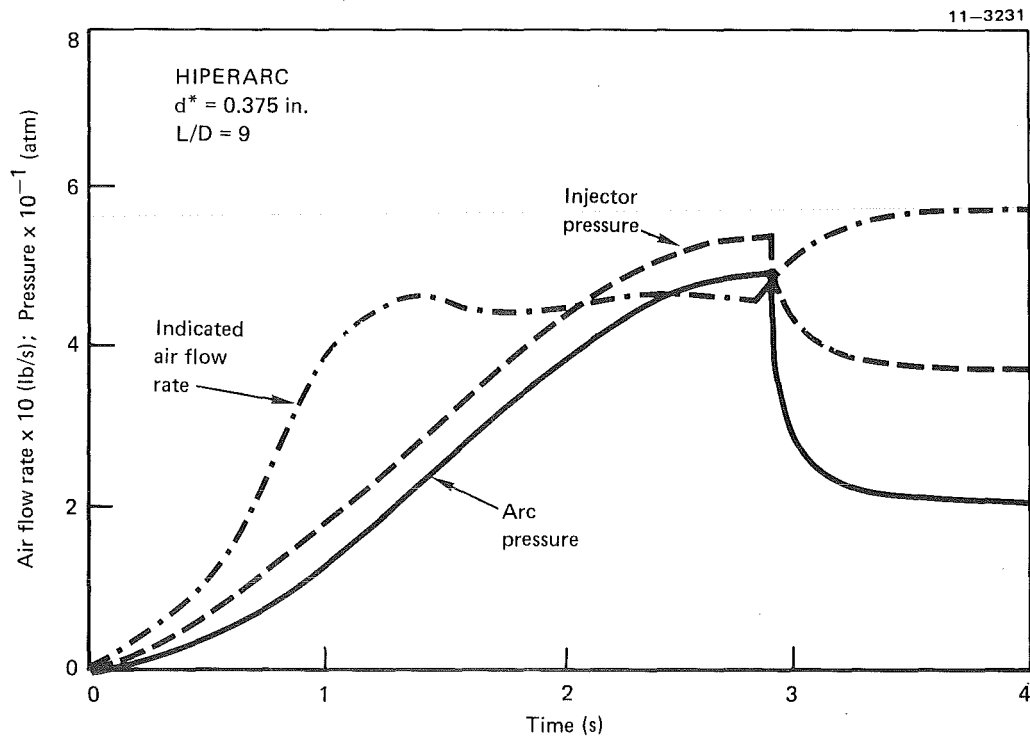
11−3231

Figure 14   Mass flow indicated — long ramp to 50 atm
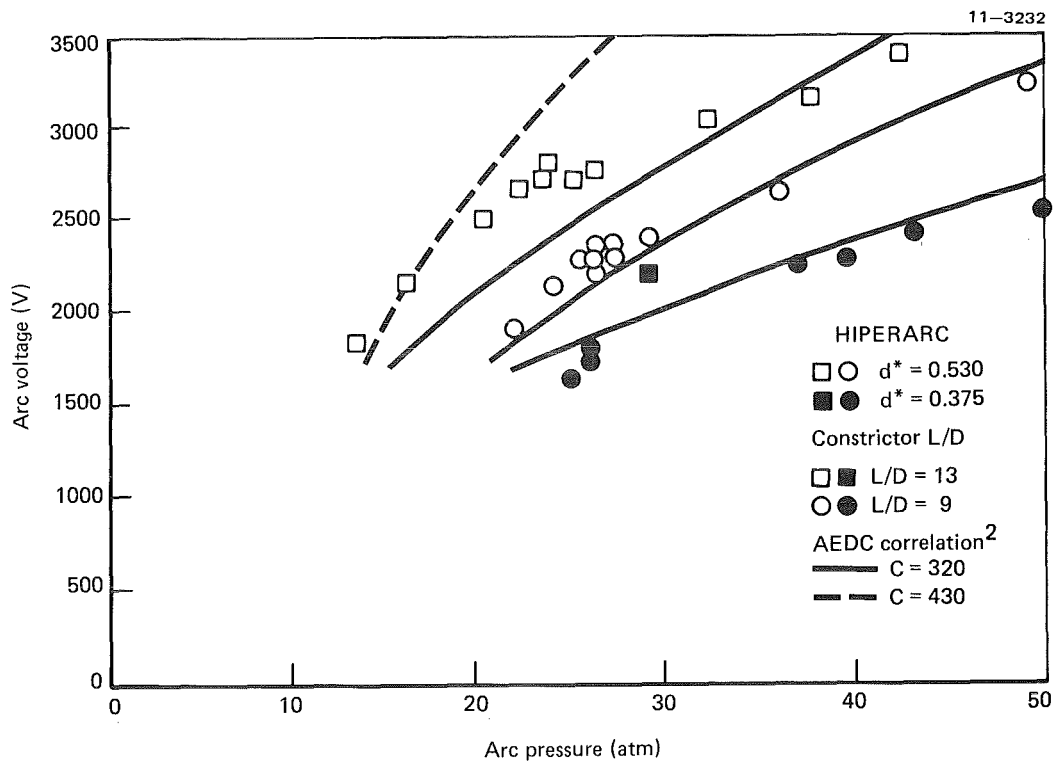
11−3232

Figure 15 Effect of arc pressure on arc voltage

Table 8 Hiperarc mass flow requirements

11—3227

Nozzle d* = 0.530 in.; constrictor L/D = 9				
Test	Arc current (A)	Arc voltage (V)	Arc pressure (atm)	Air flow rate (lb/s)
24	664	2550	38	0.79
26	557	2430	32	0.66
27	530	3160	43	0.96
32	738	3370	51	1.12
38	702	2660	36	0.72
39	666	3250	49	1.08
72	580	2320	26	0.55
73	720	2400	29	0.53
74	740	2420	29	0.53
75	740	2370	26	0.46
77	760	2270	26	0.46
78	750	2300	26	0.44
79	800	2350	27	0.46
80	800	2400	27	0.44
81	750	2350	26	0.44
82	780	2380	26	0.42
83	790	2280	24	0.37
84	830	1880	22	0.33

Nozzle d* = 0.375 in.; constrictor L/D = 9				
Test	Arc current (A)	Arc voltage (V)	Arc pressure (atm)	Air flow rate (lb/s)
142	548	1955	24	0.25
144	523	1646	25	0.25
145	550	1706	26	0.28
146	506	2268	37	0.40
149	579	1631	24	0.26
150	535	1715	25	0.24
152	496	1780	25	0.25
154	608	2453	50	0.46
Nozzle d* = 0.530; constrictor L/D = 13				
68	746	——	48	0.83
85	720	3400	42	0.64
91	584	2262	25	0.35
92	622	2285	25	0.31
94	670	2285	25	0.33
99	687	3034	32	0.46
107	700	2847	24	0.39
110	736	2719	25	0.41
Nozzle d* = 0.375; constrictor L/D = 13				
120	720	2200	29	0.24

The correlation of AEDC[2] data is shown for comparison using two values of the coefficient, C. A coefficient of 320 agrees best with the higher pressure data whereas the AEDC coefficient of 430 agrees favorably with the larger throat low pressure data. All of the data shown are for arc currents between 600 and 800 A. The effect of increased arc current normally reduces the arc voltage.

The instantaneous arc voltage may be significantly different from the average value. For a highly unstable arc the variations were as much as ± 1000 V from the average value. These variations were the result of arc spiraling, arc blow-through and arc roll-over on the anode. The larger

variations in arc voltage could be correlated between the high speed motion
pictures and the oscillograph recordings of the arc voltage. For example,
a large arc spiral added approximately three inches to the total arc length
of nine inches (short constrictor) increasing the arc voltage by one-third.
On those occasions when the arc blew through the nozzle throat, the arc
voltage increased due to the increased arc length and gas flow rate.
(The cold gas shroud around the arc passing through the nozzle reduced
the arc pressure causing an increase in the mass flow rate.) In addition
there was a 200 to 300 V secondary arc on the return path from the nozzle
to the cathode. This phenomenon was more prevalent using the large throat
and short constrictor. On numerous occasions the anode arc termination
rolled over from a rotational path on the downstream face to a rearward
location causing an increase in arc length and thus voltage. The factors
influencing arc stability will be discussed further in a later section.

The arc pressure/air flow rate influenced the visibility of the arc
column in the constrictor. As the pressure was increased from essentially
zero on start to final levels as high as 50 atm the surrounding gas varied
from perfectly clear to nearly opaque. Radiation from the arc-affected
gas was severe at high pressure, obliterating downstream events.

In summary, increased arc pressures through increased gas flow rates
decreased arc spiralling and kinking but increased constrictor intersegment
arc over, rear electrode arc roll-over, arc blow-through and arc blow-out.
Higher pressures/flow rates also increased the turbulence in the flow
changing the arc column character from a cylindrical column to a turbulent
plasma core in the converger region.

4.1.2 Circulation Effects

The primary purpose of circulating the air entering an arc heater is
to provide radial pressure forces that balance the natural arc kinking
forces and thus contain the arc column in an area away from the physical
boundary. The level of circulation required is thus dictated by the neces-
sary centripetal forces on the arc column. These forces must counteract
a combination of natural kinking forces from the self-magnetic field gener-
ated by the arc current and those superimposed by external magnetic field
coils.

The secondary purpose of circulation of the air entering the arc heater near the electrodes is to assist in rotating the arc termination on the electrode surface to prevent burnout. In addition the radial pressure gradient established by the conservation of angular momentum causes a reverse flow at the rear electrode which helps to position the rotational path of the arc on a well cooled surface.

The circulation level in HIPERARC was varied in four ways during these experiments. The mass flow rate and distribution were varied, the radius of injection for the primary gas was varied, and the injection pressure ratio was varied (ratio of injection pressure to arc chamber pressure). The experimental control and variable range for these circulation parameters are given in Table 9.

Table 9 Circulation variations

11—3213

Circulation parameter	Experimental control (range)	Variable range
Mass flow rate	Nozzle area (0.11 to 0.22 in.^{2})	0 to 1.1 lb/s
Mass flow distribution	Orifice area (see table 3)	40% to 82% primary flow
Injection radius	Injection angle (0 to 35°)	1.5 to 1.8 in.
Injection pressure ratio	Injection area (0.097 to 0.115 in.^{2})	1.03 to 1.1

40

The effects of circulation variations produced by changing the nozzle throat area were quite evident in both the motion pictures and data recordings. The reduction in mass flow rate for a given arc pressure resulting from a factor of two reduction in the nozzle throat area (compare Figs. 10 and 11) allowed the arc column throughout the heater to move outward radially from the heater centerline to a larger helix as shown in Fig. 16. Figure 16 compares two selected frames from tests using the two different nozzles for conditions of similar pressure and arc current where the circulation level varies by a factor of two. The effects of the higher circulation level in the large nozzle is apparent from the better containment. In the early small nozzle tests the reduced circulation resulted in arc-wall contact in the converger and constrictor leading to intersegment arcing and hardware destruction.
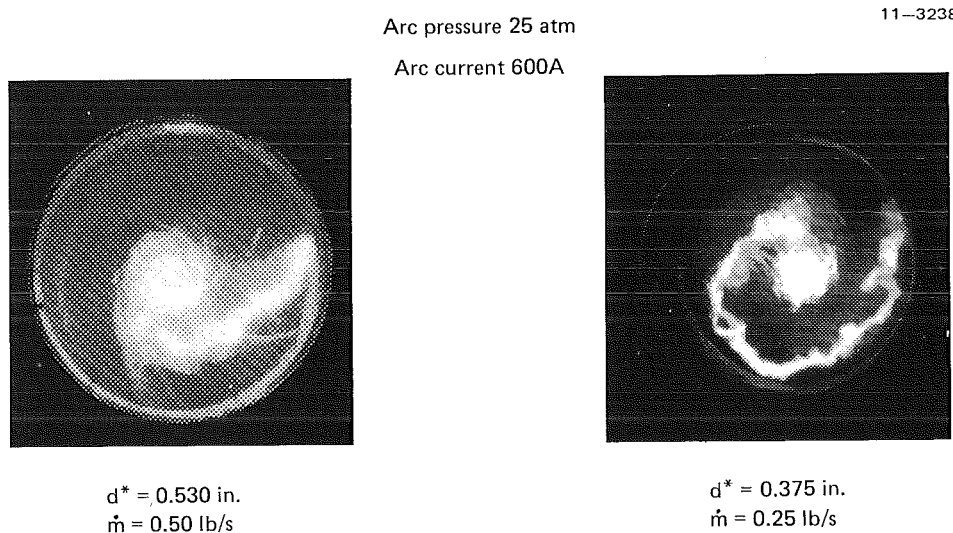
Arc pressure 25 atm

Arc current 600A

11—3238

d* = 0.530 in.
ṁ = 0.50 lb/s

d* = 0.375 in.
ṁ = 0.25 lb/s

Figure 16 Effect of gas circulation on arc stability

41

The end result of insufficient circulation is shown in Fig. 17 which is a frame taken 0.1 s after the large arc helix shown in Fig. 16 occurred. The arc current is conducted from the anode to the cathode via a series of short arcs and segment conduction in a cascade manner. Severe erosion occurs on all attachment surfaces whether they are cooled or uncooled. The gas is virtually unheated in this intersegment arcing mode.
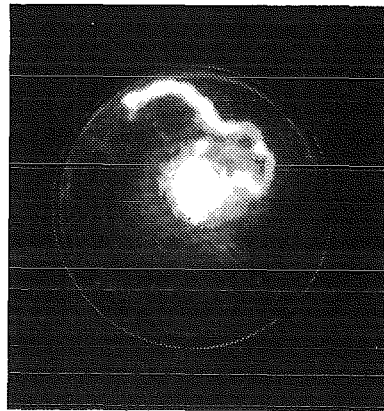
11—3237

Figure 17 Intersegment arc over resulting from insufficient circulation

The effect of a limited variation of injection radius on the circulation level was investigated in an attempt to stabilize the arc using the small nozzle. The 16 injectors located between the anode and first converger segment were nominally 0.0625 in. diameter. All of the tests through No. 122 were made with these injectors drilled tangential to the anode flange radius, i.e., 1.83 in. (Fig. 1). The strong flange scrubbing effect of this injection resulted from the direct impingement of each jet on the flange and suggested potentially large frictional losses. The angle between the injector centerlines and the flange circumference was changed to 35 deg yielding an effective injection radius of 1.5 in. for all tests after No. 122. Although this radius reduction in a freely circulating flow would reduce the specific angular momentum, the avoidance of strong frictional losses in a contained flow should more than compensate and in fact lead to a stronger circulation.[1] The arc behavior with the modified injection radius indicated an increased circulation was achieved.

The arc location moved rearward on the toroidal anode and the intersegment arcing was reduced. This variation was definitely beneficial to the arc location and stability but by itself was insufficient to totally prevent intersegment arcing.

The gas injection velocity is related to the inverse of the injection pressure ratio in the following manner for a given gas temperature: [8]

$$v_i \propto \left[r^{2/\gamma} - r^{(\gamma+1)/\gamma} \right]^{1/2} \tag{3}$$

where v_i = gas injection velocity,

r = inverse injection pressure ratio (P_o/P_i), and

γ = ratio of specific heats = 1.4

From this relationship it can be seen a very modest increase in the injection pressure ratio from 1.03 to 1.10 produces a 75% increase in injection velocity and thus circulation. Persistent intersegment arc-over when using the small nozzle prompted experiments that realized such an increase.

The injection pressure ratio of HIPERARC was increased from 1.03 to the 1.08-1.10 level by removal of 12 constrictor segments and their associated injection area. In so doing, the remainder of the arc heater (including the nozzle throat area) did not require any changes. The increased injection velocity had a definite stabilizing effect on the arc and, when used in conjunction with a reduced rear electrode spin coil field strength, provided the necessary stability to conduct experiments on other variations.

The best evidence that a higher injection velocity would yield improved stability was noted during the early phase of each test conducted. The injection pressure ratio exceeded two at the start of a test when the arc chamber was virtually cold and the back pressure on the injectors was minimum. Under these conditions the injection velocity started out sonic and diminished to the final level which was insufficient. At the higher velocities the arc was very stable and tightly contained at the heater center but as the velocity diminished large arc spirals would develop, leading to intersegment arcing.

4.1.3 Air Flow Distribution Effects

The variations in air flow injection distribution for these experiments
are presented in Table 3 (p. 15). The physical location of these gas injec-
tion stations is shown in Fig. 1 (p. 3). The observed effects of these varia-
tions were sometimes subtle and sometimes dramatic. The following discussion
will attempt to delineate the individual or unique effects of each injec-
tion station starting at the rear of the heater and proceeding forward
to the nozzle. The conclusions or observations are general in nature
since quantitative effects are extremely difficult to measure.

A low percentage (< 2%) of the total gas flow was injected at the
rear window to prevent obstruction of the camera view into the heater.
It was found that for all cases except during disastrous intersegment
arcing (with resultant contamination) that the flow was adequate to prevent
obscuration.

The injection station at the rear of the rear electrode (rear retard)
proved to be important in preventing the arc termination (normally the
anode) from attaching to the first rear isolator and thus causing an insta-
bility. Rear retard variations from 3 to 11 percent of the total flow were
tested. At the lower levels there were persistent excursions of the anode
to the isolator as noted both on the films and on the isolator voltage
recording. This occurred only in those tests where the general anode location
was rear of the torus midplane. Increasing the rear retard flow eliminated
attachment to the isolators without causing significant general anode
location changes. For those tests where the anode location was forward
of the torus midplane, reductions in the rear retard flow had no signifi-
cant influence.

The highest percentage of gas flow at a single axial station was
consistently injected between the rear electrode and the converger through
16 holes of 0.0625 in. diameter. As discussed previously, the angle of
injection was varied from tangential to the flange circumference to 35 deg
off tangent. In addition the percentage of the total flow at this station
was varied from 27 to 61 percent.

It was observed that arc stability was enhanced at the higher rear
electrode gas flow rates, particularly in the converger. The arc spiral-
ing was reduced and for those cases where instabilities did occur they were
delayed until later in the start cycle. The arc location on the rear
electrode was an indicator of the amount of reverse flow, and in general,
that location was moved further to the rear by an increased gas flow per-
centage at this station.

In an early series of tests (No.'s 107-110) the gas flow percentage at the
rear electrode was reduced from 39.2 to 26.7 percent in two steps. The arc
current oscillations and arc instabilities, i.e., blown arc and arc kinking
were significantly more severe as the percentage of gas flow was reduced
at the rear electrode. Table 10 summarizes the conditions and observations
for these variations.

Table 10 Some effects of flow distribution

11—3214

Test no.	107	109	110
Nozzle diam. (in.)	0.53	0.53	0.53
Arc current (A)	600—750	540—720	530—750
Arc voltage (V)	2000—2500	2200—3100	2400—3500
Arc pressure (atm)	24	23	24
Rear electrode flow (%)	39.2	33.3	26.7
Primary/secondary flow	60/40	50/50	40/60
Stability	Good	Fair	Poor
Blown arcs	None	Several	Few
Inter-segment arcs	None	None	None
Roll-over arcs	None	Several	Few

The percentage of the gas flow injected in the converger region was
approximately one-fourth of that at the rear electrode for all tests.
Thus, independent effects of the converger gas injection were not deter-
mined. It was observed in those tests where inter-converger-segment
arcing occurred, that the individual arcs in the segment gaps were not
rotated nor blown out by the intersegment gas flow.

The total gas flow injected upstream of the constrictor (primary flow)
has less effect on the arc rotation rate than expected. Figure 18 shows
the arc rotation rate for 40 and 60 percent primary flow with the large nozzle
and 60 and 80 percent with the small nozzle. The rotation rate is a little
higher for the large nozzle (twice the flow rate) and slightly higher for
the higher primary flow. However, the only significant differences occur early in

45

the test when the injection pressure ratio is highest and thus the gas
velocity is maximum. The decaying injection velocity combined with increased
retrograde forces causes a decay in the rotation rate until very near the end
of the test where the higher arc current begins to increase the rotation
rate. This occurs since the Lorentz force with the series field used in
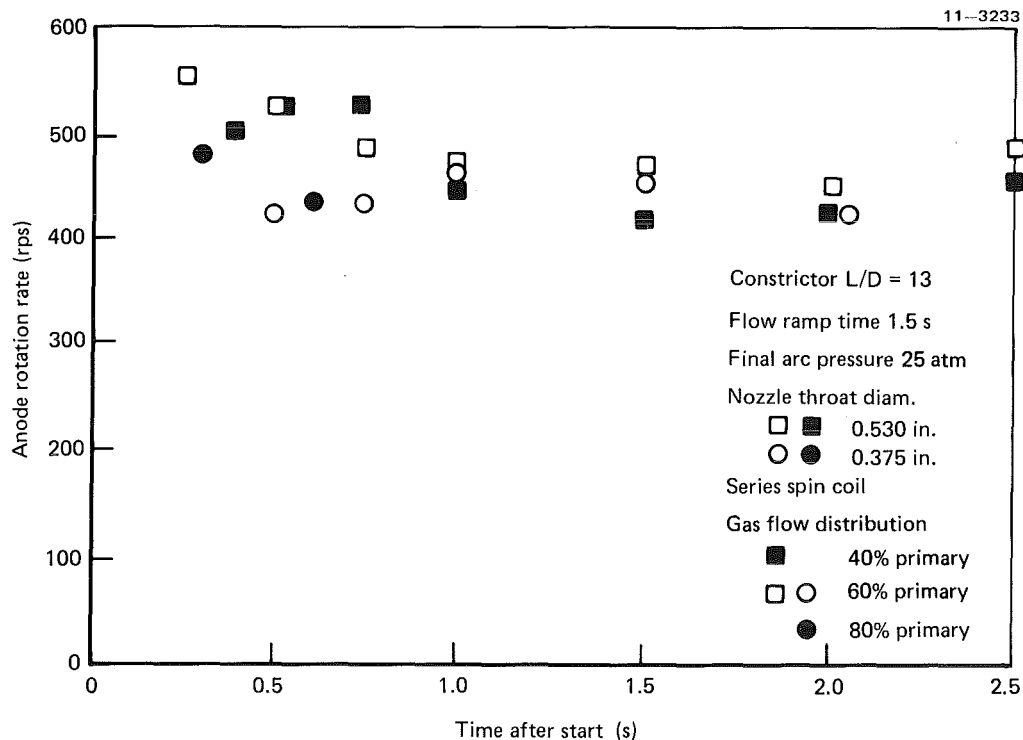this test is proportional to the arc current squared.

Figure 18 Effects of circulation on anode rotation rates

The amount of flow divided evenly among the 24 constrictor segments
for L/D = 13, was varied from 38 down to 10 percent in an effort to alleviate
intersegment arcing with the small nozzle. The result was opposite that
expected, i.e., the problem was more severe at the low constrictor flow
rates. Since the damage from each test further roughened the segments, there
is cause to believe the noted effects were not entirely attributable to gas
flow variations.

The quarter torus shape of the forward electrode in HIPERARC provides
a deceleration of the gas flow encouraging the arc to attach to the electrode
wall. The physical arc length from the electrode entrance to the toroidal
surface can be the order of 2 in. Thus, when the last constrictor segment

46

assumes the potential of the local arc column it creates a significant
potential difference from the immediately adjacent electrode entrance.
For this reason the amount of gas flow at this gap must be significantly
higher than other constrictor segment gaps to prevent arc-over. The
percentage of the total flow injected at this front slot was varied in
these experiments from 0 to 10.9 percent. The effects of this flow variation
are best illustrated in a comparison of tests 107 and 109 where the front
slot percentage of the flow was increased from 3 to 10.9 percent. At the
low flow rate the last segment assumed the same potential as the cathode
indicating arcing to that segment. In the higher flow test, the last segment
rose to a level 400 V above the cathode and no arcing occurred to the
segment.

The purpose of gas injection between the forward electrode and the nozzle
is primarily to prevent the cathode attachment from wandering into the insulator
gap. The forward electrode is electrically tied to ground through a 2 kΩ
resistor and the nozzle is grounded to eliminate electrical noise to diag-
nostic probes. A potential difference up to 300 V has been measured
between the two components in normal operation. Thus the secondary purpose
of the front retard flow is to prevent arc blow-through and arc back between
the nozzle and forward electrode. The front retard flow rate was varied
from 1.5 to 6.3 percent of the total gas flow in these experiments. The
tendency for arcing to the nozzle and arc-back to the cathode was greater at
the low flow rates. This was observed through the forward electrode potential
data and by visual inspection of the nozzle entrance.

4.1.4 Starting Ramp Effects

Starting the arc in a high performance arc heater is relatively simple
but transitioning from arc breakdown to the desired arc pressure and current
must consider several factors. Such considerations include the power supply
response characteristics, the circuit inductance, circuit resistance, gas
flow control response and interlock precautions.

The normal start procedure for HIPERARC in LCAT was presented in Section 2.2
(p. 5). A typical oscillograph recording of the component potentials, arc
current, injector pressure, arc pressure and interlock information is shown

in Fig. 8 (p. 23). The transition can be followed from right to left. Arc breakdown at an arc pressure less than 10 Torr results in a high current surge which decays rapidly to a low level (200-400 A) for a short period then slowly increases to the pre-set level. The arc voltage remains at a low level until the gas flow arrives in the heater. The initial abrupt voltage increase is caused by the pre-load on the fast acting ball valve in the air line. As the regulator is loaded at a pre-set rate, the air flow rate and arc voltage increase in a regulated manner to their final levels. The natural arc characteristic would decrease the arc current as the voltage increases but simultaneously the saturation current to the power supply reactors is being increased so there is a net increase in arc current despite the increasing voltage. If the ramp rate is too fast, the arc current will decrease causing arc blow-out. If the ramp rate is too slow, the arc current will reach its maximum before the full gas flow and this can lead to intersegment arcing.

The segment potentials (i.e., converger, constrictor, and isolators) can be seen in Fig. 8 (p. 23) deflecting downward to a positive voltage. The response of the converger and constrictor segments as a function of their resistance to ground is discussed in Section 4.2.4 (p. 53). In general, their potential normally increases in the entrance region on start then decreases as the cold shrouding gas is established. The potential of the downstream segments gradually increases throughout the start ramp as more charged particles drift to their surfaces. Sharp increases in the segment potentials followed by a decrease in arc voltage and an increase in arc current signified intersegment arcing and this was correlated very closely with the filmed data. These filmed experiments have made identification of intersegment arcing an easier task requiring only the oscillograph recorded data.

The ratio of the injector pressure to the arc pressure is an indicator of the gas injection circulation level. The oscillograph recordings indicate that the initial injection pressure ratio is greater than two and thus the injection velocity is sonic. At the end of the start ramp the injection pressure ratio has decayed to very low levels (1.03 to 1.1) and the injection velocity is low subsonic. It was apparent from the films

48

and data records that the arc stability was greatly enhanced by the higher injection velocity. The arc was better centered and the rotation rates were much higher. Modifications to the gas injection area beyond those tested here are needed to enhance the final injection pressure ratio and ensure stability.

Two arc power interlock signals shown in Fig. 8 (p. 23) can be used to avoid hardware damage from intersegment arcing. The inactive interlock signal from a photocell in the exhaust region was quite sensitive to intersegment arcing, contamination and blown arcs. This system deserves further development. The arc voltage interlock was triggered by the aforementioned decrease in arc voltage with intersegment arcing. The problem with this interlock is that it can not be activated until the arc voltage is above a pre-set level. Thus, it is sensitive to the ramp rate. Normally, the system was activated 1.1 to 1.7 s after arc initiation depending on the ramp time.

The starting ramp time was pre-set with a needle valve controller in the load line of the primary gas regulator. The time was checked before each test using a cold flow ramp. The start ramp time was varied from 1.0 to 2.0 s in these experiments with the normal range from 1.2 to 1.7 s. The shorter times were used at lower arc pressures and the longer ones at the higher arc pressures.

The effects of starting ramp time are primarily stability effects. As previously stated, if the ramp is too fast, the arc current has not yet started its ramp and the high voltage demand from severe arc kinking and extension aggravate the situation leading to arc blow out. If the ramp rate is too slow then the arc current reaches full value before the gas flow rate and this can lead to intersegment arcing. In addition, a slow ramp delays the activation of the interlock circuit which places the hardware in jeopardy. Within the proper range (1.2 to 2.0 s for HIPERARC in LCAT) the ramp time is not critical. If the time is not extended for higher flow rate tests, the anode spot can be blown off the rear electrode on to the isolators causing instabilities. Each arc heater and power supply will have a unique ramp time range that must be established experimentally.

4.2   ELECTRICAL CONTROL EFFECTS

The electrical arc control variables in these experiments included the arc current, the level and mode of spin coil excitation, the arc polarity, and the resistance between the converger-constrictor segments and ground.   Observations from previous HIPERARC experiments[5] are included for completeness.

4.2.1   Arc Current Effects

In a typical HIPERARC start (Fig. 8), the arc current spiked to 800 A then decreased to the order of 300 ± 100 A in less than 0.1 s where it remained constant until the gas flow entered 0.3 s after breakdown.   The current then decreased to the order of 240 A before gradually increasing to the pre-set level.   Normally the final value was reached in a time interval approximately equal to the gas ramp time.   Since the saturation current to the power supply reactors was pre-set, the final current was dependent on the arc voltage and thus the gas flow rate.   This caused the arc current to change through the arc start-up, which usually lasted for 1.5 s.   It was found that start times under 1.0 s resulted in arc blow-out since the voltage demand overrode the ability of the power supply to respond causing a decrease in arc current and arc elongation.

In general, higher arc currents increased the high enthalpy core size which is desirable for high performance.   However, higher arc current increased the electrode erosion and the constrictor heat flux.   Instabilities resulting from self-magnetic fields and interactions with spin coil fields were aggravated by higher arc currents.   On the other hand, it was observed that arc kinking (not spiralling) was less than at low arc currents.

Figure 19 shows the effect of arc current on the arc column diameter near the anode for three pressure levels.   These data were acquired at the end of the tests where the pressure and gas flow rate were nearly constant. The 12 atm data indicate an arc column cross-sectional area that is nearly proportional to the arc current whereas the 17 and 23 atm data indicate the arc diameters increase linearly with arc current.   All of the measured arc diameters were less than 4.1 mm which is smaller than the 6 to 10 mm diameter predicted by the SWIRL ARC code for a 700 A, 25 atm condition.
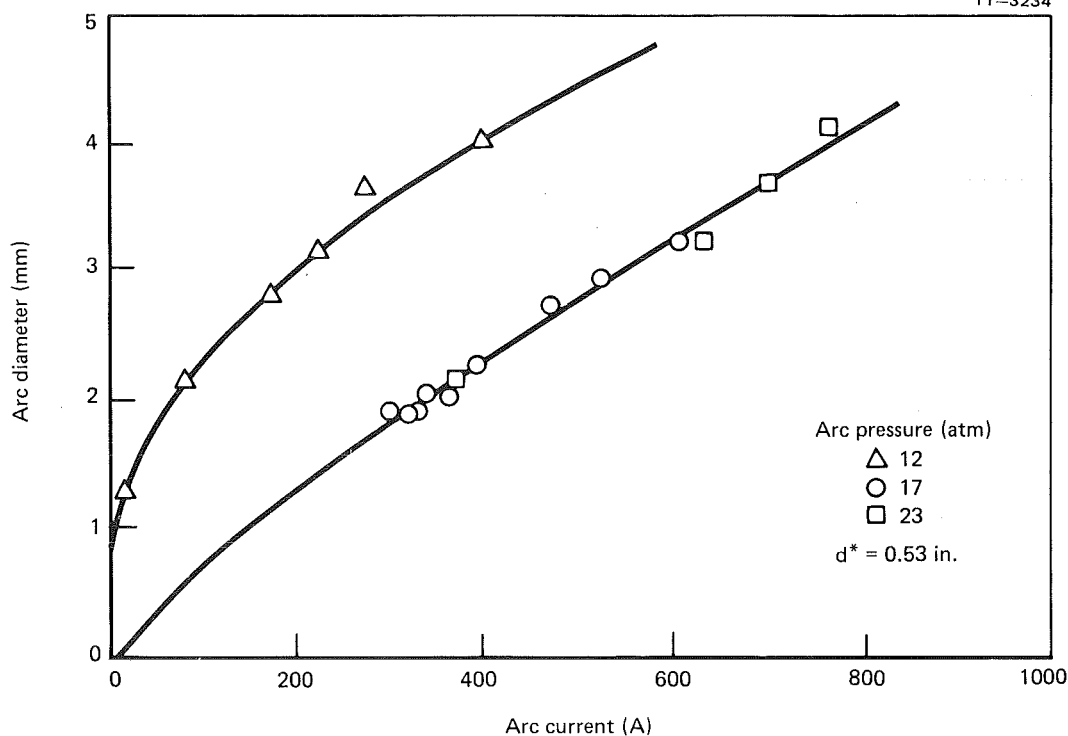
Figure 19 Effect of arc current on column diameter

Figure 20 is a sequence of frames from test 109. The effect of arc current is apparent as the level decreases from 750 A to 300 A. The rear arc spiral is greater at the high current indicating a higher probability of intersegment arcing. The local arc kinking is greater at the low current levels but the column is better contained as a whole.

4.2.2 Spin Coil Excitation Effects

Two series of tests were conducted wherein the rear electrode spin coil was separately excited by a dedicated power supply. In this way, the Lorentz force was directly proportional to the arc current instead of being a complex function of the arc current squared and the rate at which it was changing. In addition, the separately excited field strength could be reduced without a major hardware change for a given arc current.

The separate spin coil excitation tests were initially conducted with the small nozzle (0.375 in.), an L/D of 13, and a flow distribution of 60 percent primary and 40 percent secondary. The pre-set saturation current was 86 percent and the pre-set gas flow pressure was adequate to yield 30 atm pressure on full condition.

51
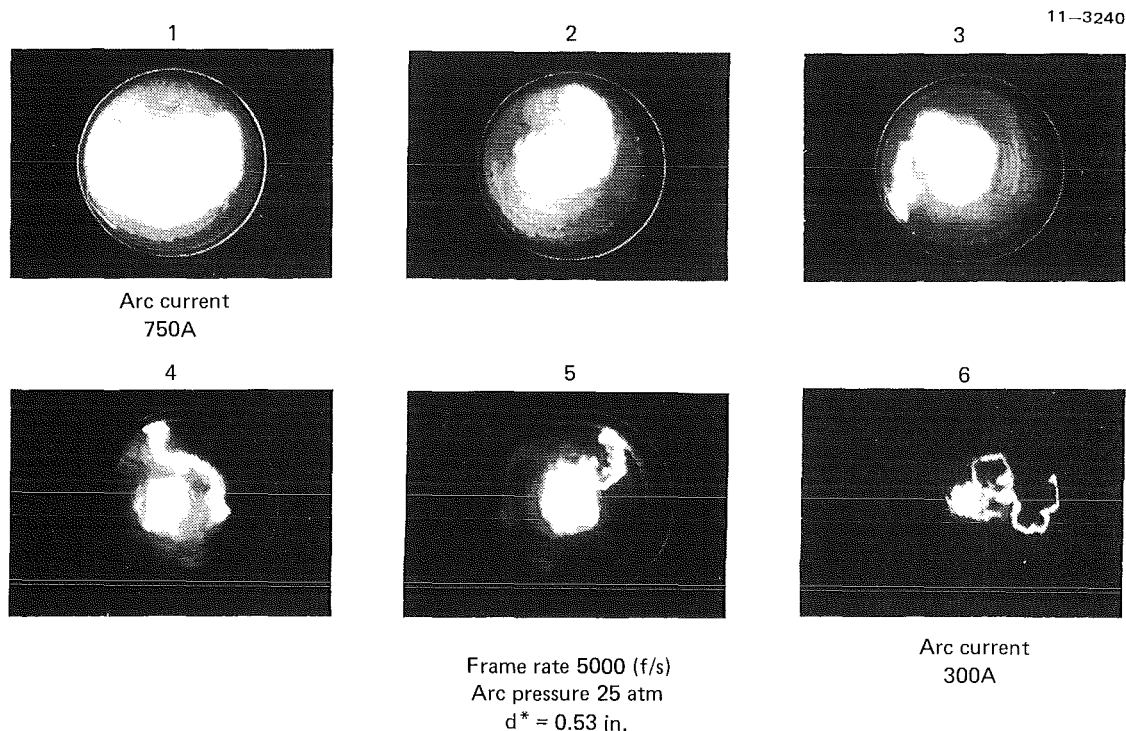
Figure 20 Effects of arc current on column shape

The three previous tests using a series coil with this same configuration and condition had been of marginal stability with terminations of the test by one of the interlocks upon minor intersegment arcing. The arc spiral in the converger was being enlarged by the interaction of the circumferential current and the axial field. It was reasoned that a reduction in the field strength should reduce the spiral radius and enhance stability. This proved to be true.

A preliminary test with the separately excited coil was made to establish the required interlock voltage and check the spin coil insulation. The next two tests (No.'s 127 and 128) exhibited the highest stability achieved to date using the small nozzle. The arc current was 570 $\pm$ 30 A and the arc voltage was 2000 $\pm$ 200 V. There were no indications of intersegment arcing. An increase in the rear retard gas flow rate in test No. 128 from 3 to 7 percent of the total flow eliminated the minor isolator arcing experienced in test No. 127. The arc pressure in both tests was 29 atm.

The spin coil current was 400 A throughout these initial tests. The lower field strength reduced the arc spiral radius in the converger region and significantly enhanced stability. The balance between the inward

radial pressure forces from the swirling flow and the outward Lorentz forces occurred at a smaller radius. These tests also illustrated that improved circulation would further enhance stability.

A second series of tests was conducted with a separately excited rear electrode spin coil using the small nozzle and an L/D of 9 for improved circulation. The spin coil current was varied from 400 A down to 300 A. The stability of operation was increased significantly with the reduced field and improved circulation. The arc spirals in the converger were reduced and intersegment arcing was avoided. Variations in arc polarity, segment grounding resistance, and arc pressure were accomplished with the low current separately excited coil which had not been possible with the series arrangement.

In general the arc rotation rate was reduced by the lower field strength and the arc tracks on the rear electrode were more sporadic and deeper. There was, however, no significant electrode damage.

Figure 21 compares the anode rotation rates using series and separate coil excitation and shows the effect of the separate spin coil current level. The final rotation rate is nearly proportional to the coil current for separate excitation but less sensitive to current early in the tests.

The effects of several variations on the arc rotation rate are shown in Fig. 22. The arc pressure (air flow rate) has virtually no effect on rotation rate which indicates the Lorentz forces dominate the rotational drivers. As expected, the segment grounding resistance had no effect on the arc rotation rate. Reversing the arc polarity caused a sharp decrease in the initial arc rotation rate. By 0.75 s into the start, the rate was comparable to that of standard polarity. This differs somewhat from the series coil reverse polarity behavior from earlier tests. The rotation rate was slower throughout those tests. This was not due to gas injection since the gas injection direction augmented the rotation of the arc column in the amperian direction for all tests conducted.

The decay of the arc rotation rate shown in Fig. 22 can be attributed to a decrease in the gas injection velocity and an increase in the retrograde forces on the arc anode. As the arc pressure increases in the heater,
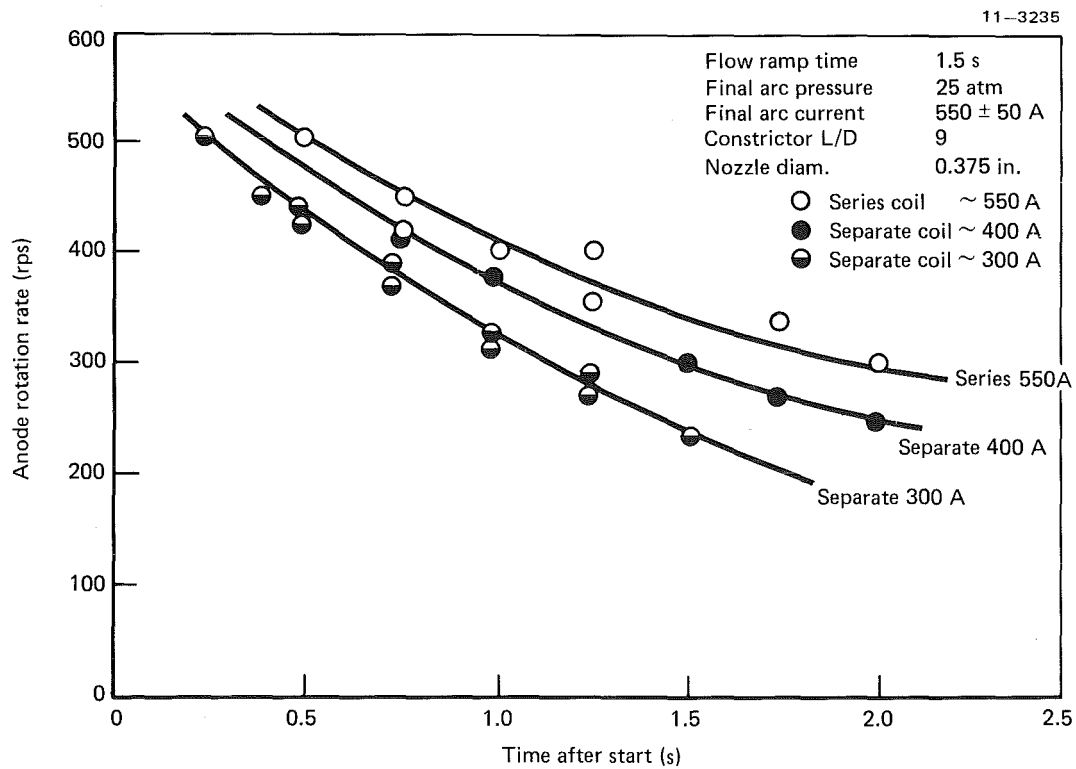
11-3235

Figure 21 Spin coil effects on anode rotation rates
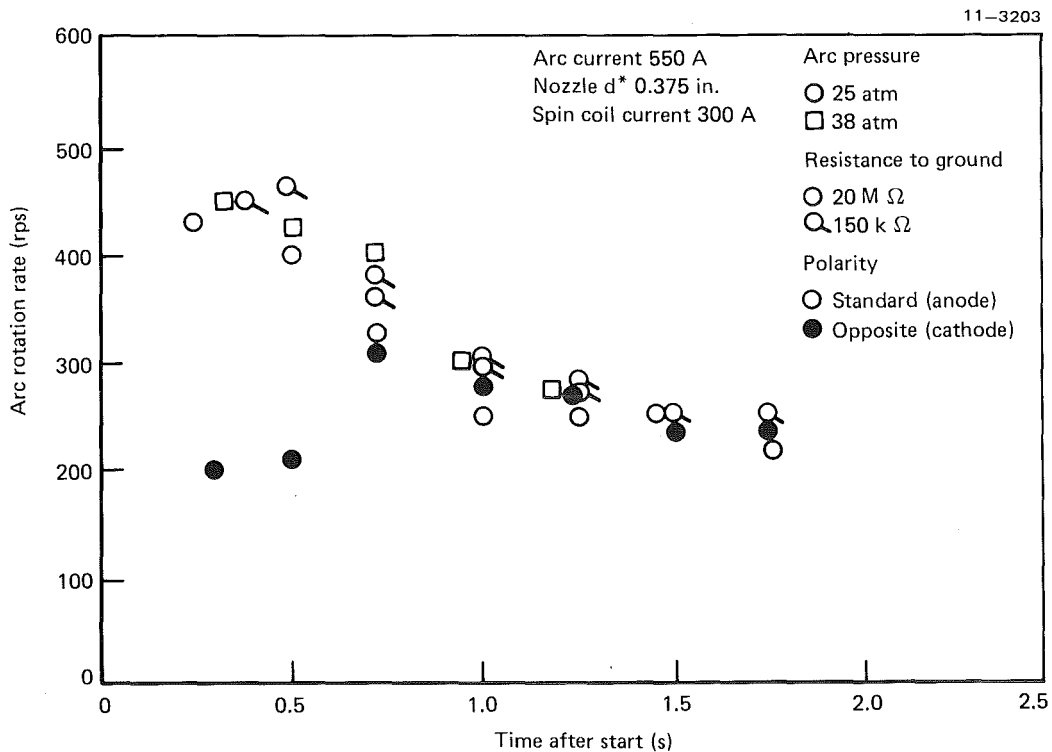
11-3203

Figure 22 Effect of control variations on arc rotation rates

54

the injection pressure ratio decreases thereby decreasing the gas velocity significantly. The gasdynamic drag on the column is proportional to the velocity squared. In addition the higher pressure reduces the arc foot size and the arc current increases with time. These combined effects yield higher current densities and stronger retrograde or retarding forces on the arc.[9] These decaying factors apparently override the accelerating effects of increased density and increased Lorentz forces. A comparison of Figs. 21 and 22 with Fig. 18 indicates the decay is reduced by the series coil with stronger Lorentz forces that introduce spiralling instabilities.

4.2.3 Arc Polarity Effects

In order to determine the effects of arc polarity a series of tests was made wherein the polarity was opposite that normally used in HIPERARC. Normally the rear electrode is the arc anode and the forward electrode is the arc cathode.

Test No.'s 113 through 115 were conducted with opposite polarity from normal using the same configuration and pre-test settings as test No. 107 i.e., the nozzle throat diameter was 0.53 in., the L/D was 13, the initial flow division was 60 percent primary and 40 percent secondary, the ramp time was 1.5 s, and the current pre-set was 86 percent of full saturations. In test No. 113 the arc blow out when the gas flow reached the heater interior. The second test (No. 114) was more successful but did not reach the desired condition, i.e., 700 A and 25 atm. After 1.1 s the arc current had reached 400 A and the pressure was 16 atm. At this point the arc voltage oscillations were as much as 1000V and the level was increasing from an average of 2500± 300V to 300 ± 500 V. This resulted in arc excursions through the nozzle throat and arc blow-out. From the films the voltage oscillations were identified as arc elongation spirals to near the injection radius at the rear electrode combined with arc roll-over to the rear isolators. An analysis of the spin coil field-arc interaction did not reveal any significant differences as a result of polarity reversal since the field directions were also reversed (series coil). The low arc current certainly contributed to the instability but the reason for the low current was not apparent.

Two problems were noted in test No. 114. There was apparent arc blow-through and the forward electrode potential (with respect to ground) was zero. Both of these problems were attributed to an internal short between the nozzle and the forward electrode. The front retard flow rate (between the nozzle and front electrode) was increased from 1.5 to 8 percent of the total flow in an attempt to retain the anode on the forward electrode instead of the nozzle.

A third test (No. 115) was then made at the same conditions. The result was not positive. The arc behavior was modified by the reduced primary gas flow (increased secondary). The cathode attachment was on the forward face of the rear electrode for the first 0.6 s (Fig. 23a) at which time it rolled over to the rear (Fig. 23b). The arc current reached 420 A before arc extensions caused blow-out. Upon blow-out an external arc ignited the main bolt insulators causing significant damage. Further opposite polarity tests were terminated in favor of small nozzle tests.

Two successive frames from test No. 115 (Fig. 24) show the arc cathode and the way it changes locations. As the arc spirals around the interior of the toroidal electrode, a shunt occurs in a new location and the previous cathode is marked by a high temperature cloud of copper. The arc rotation rate was slower with this polarity partially due to the lower arc current and partially due to the cathode thermionic emission requirements. The slower rotation resulted in deeper erosion pits on the rear electrode (Fig. 25) back quadrant.

The surface of the rear electrode (cathode) after test No. 115 is shown in Fig. 25. The bright spots were unique to these opposite polarity tests. The surface was rougher than normal. The downstream side of the rear electrode is shown in Fig. 26. The uniform discoloration occurred during the first 0.6 s of the tests at the low flow rate condition. The arc shifted to the rear at that point in the tests. This behavior was unique to the opposite polarity tests with the large nozzle.

The general conclusions from these initial opposite polarity tests with the large nozzle are not favorable. The arc rotation rate was slower aggravating erosion and the tendency for the arc to spiral, extend, and blow out were greater. These negative characteristics were partially due
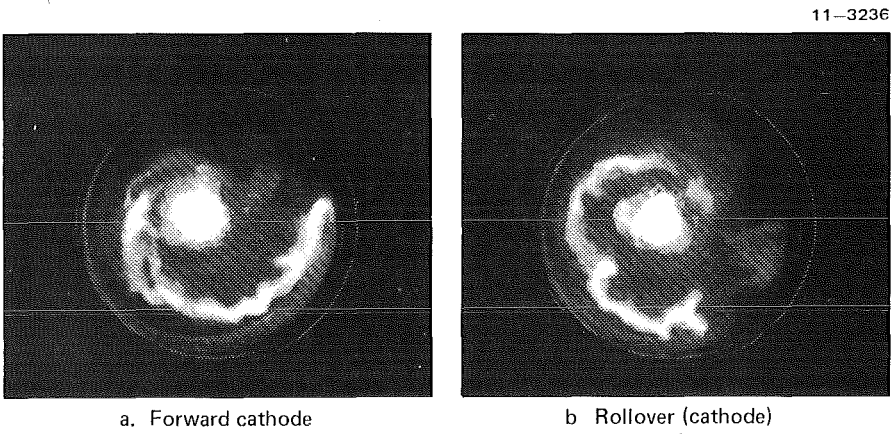
11–3236

a. Forward cathode

b Rollover (cathode)

Figure 23 Arc roll-over with opposite polarity

1 2 3 4 5 11–3239
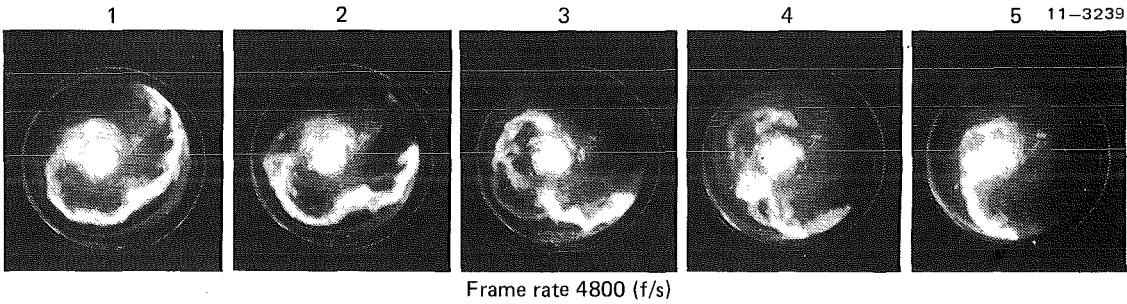

Frame rate 4800 (f/s)

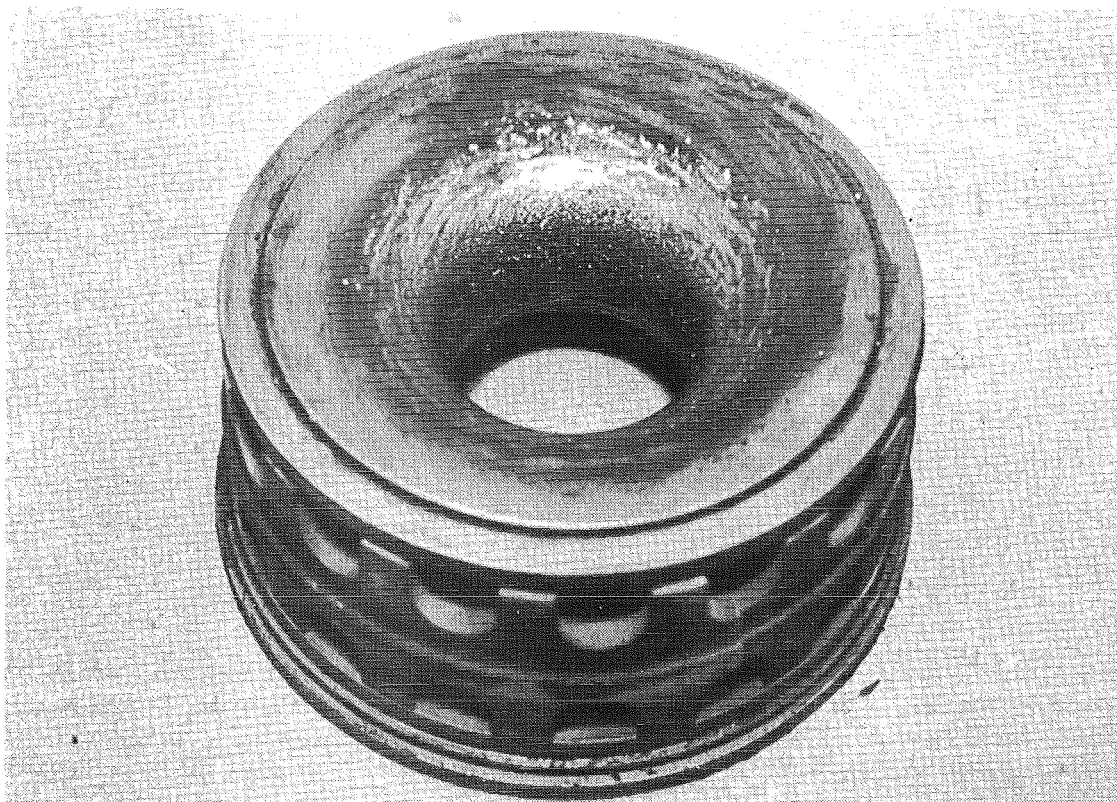Figure 24 Cathode behavior at the rear electrode

57

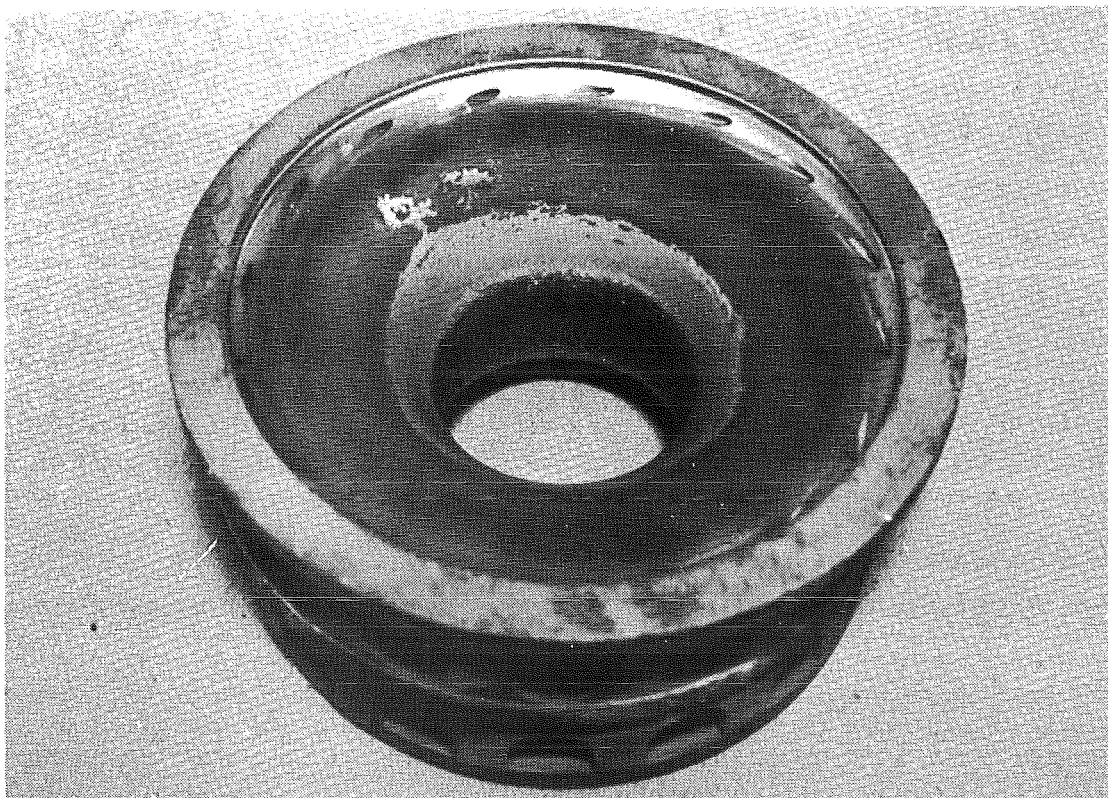Figure 25. Rear electrode after opposite polarity (rear)

Figure 26. Rear electrode after opposite polarity (front)

to a lower current arc and an internal nozzle short. The increased rear electrode erosion when it was the cathode was apparent from the copper clouds in the cathode vicinity and the pitting of the surface. There was no apparent difference in the performance parameters, i.e., voltage-pressure with opposite polarity. It should be noted that the field coil on the rear electrode in these initial tests was reversed to maintain an augmenting field for both polarities.

A second configuration was tested with opposite polarity. This configuration had a 0.375 in. nozzle and an L/D of 9. The rear electrode spin coil was separately excited at a low level (300 A). The arc was very stable except for a brief arc to segment 7 (last converger segment) early in the start which subsequently dissipated. The total arc voltage was identical to the standard polarity for the same pressure and current. However, the arc did shift slightly since the front electrode potential with respect to ground decreased from 150 to 0 V. Again, as with larger throat tests, the arc residence time was longer on the rear electrode and similar cathode jets of copper vapor were visible.

It appears there is very little effect of polarity on heater operation except for the increased erosion of the toroidal rear electrode. Longer tests would be necessary to quantify this difference.

4.2.4 Segment Grounding Resistance Effects

Tests were conducted to determine the effects of segment to ground resistance on arc stability. The converger and constrictor segments in these tests were uncooled and thus the resistance between them and ground could be fixed using wire wound resistors. The natural resistance to ground exceeded 20 MΩ and most of the tests were conducted at this level. Previous tests[5] had been made using 300 and 150 kΩ grounding resistors but no high speed films were taken in those tests. The present tests were made with >20 MΩ and 150 kΩ to provide relative arc behavior for otherwise identical conditions.

The electrical resistance between the column in a constricted arc and ground determines the level of radial or drift current away from that column. This resistance is the sum of the gas resistance between the

arc column and the constrictor wall and the resistance between the constrictor segment and ground. The former is dictated by arc heating phenomena and the latter is generally fixed by the cooling water connections to the segment. Realistic levels for the latter range between 100 and 500 kΩ.

The potential of a constrictor segment during proper operation is determined by:

$$\frac{V_w}{V_a} = \frac{R_g}{R_a + R_g} \, , \qquad\qquad (4)$$

where V_w = segment potential,

V_a = local arc potential,

R_g = resistance between segment and ground, and

R_a = resistance between arc column and segment.

The local arc voltage is nearly a linear function of the distance rearward from the cathode. Thus the segment potential can be estimated if the relative resistance levels are known. The SWIRL ARC code[6] predicts the value of R_a and for an input R_g will calculate V_w/V_a. Figure 27 compares the measured component potentials from previous tests[5] with the predictions from SWIRL ARC.[6] In the entrance or converger region the cold gas insulates the wall. As the gas mixes with the arc heated core, the electrical resistance between the arc column and the wall decreases dramatically and the segment potentials rise to near that of the arc column. A reduction in the segment to ground resistance delays the transition to a position farther downstream. It is apparent that a high potential difference between the arc column and wall exists over a much greater length in the constrictor with the lower grounding resistance. This makes the constrictor more susceptible to arc shunting and intersegment arcing. The effective conductivity of the gas shrouding the arc column is shown in Fig. 28 for conditions typical of many of the tests conducted during this effort. The conductance changes nearly four orders of magnitude over the arc length. These data were derived from the inverse gas resistance from Eq. (4) using measured segment potentials and total arc voltages. The resistance between
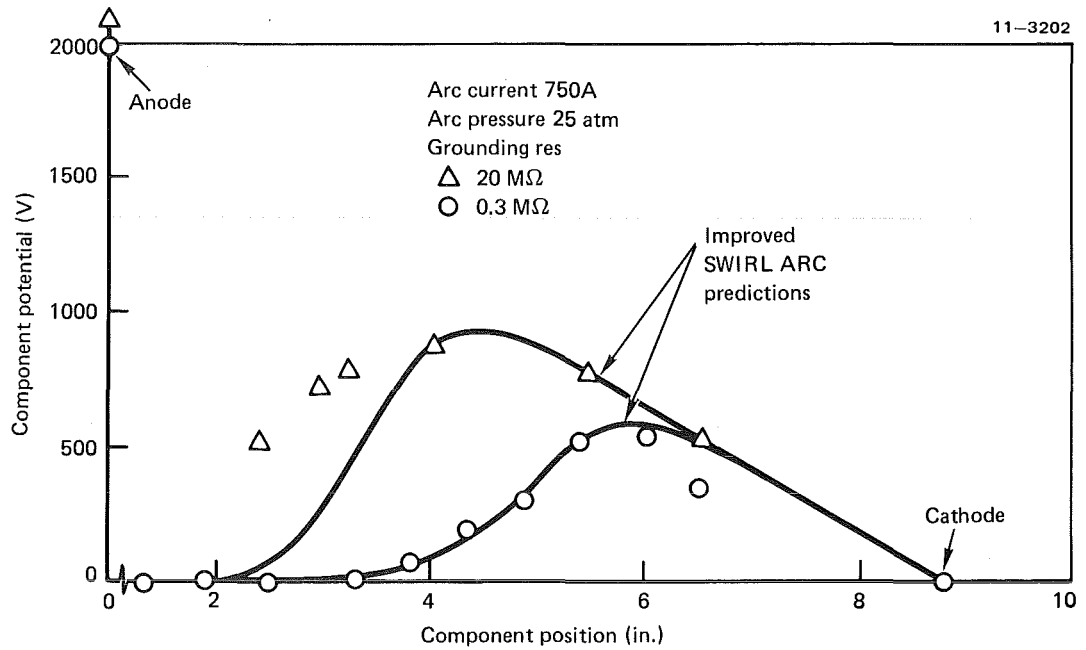
Figure 27 Comparison of measured and predicted HIPERARC component potentials
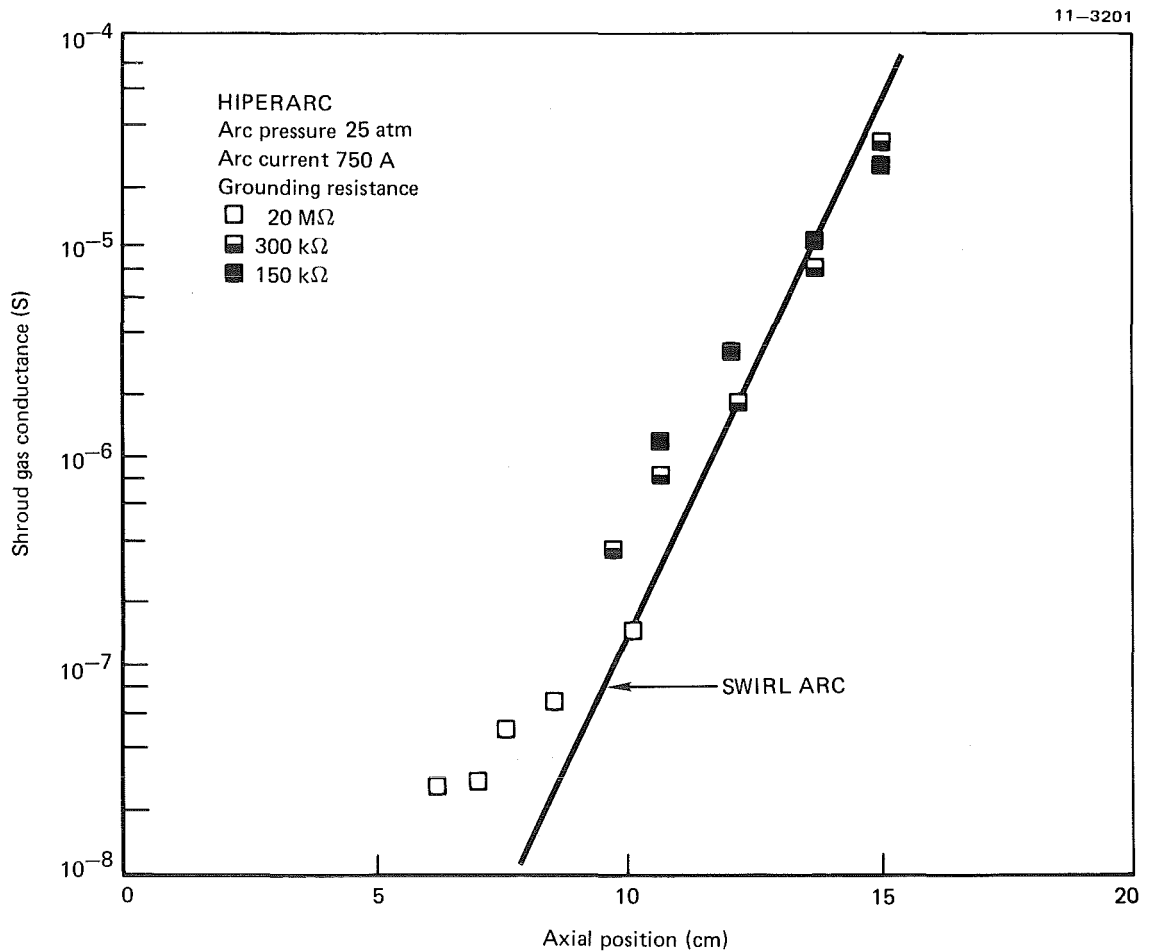

Figure 28 Arc shroud gas conductivity

the segment and ground is shown in the figure. The location of each data
set is dictated by the potential transition region for that resistance.
The predicted effective conductance is shown for comparison. Agreement
is reasonably good in the constrictor where the diameter is the same for
both the prediction and the data. The code does not allow for the varia-
tion of diameter in the converger.

Figure 29 compares the segment potentials measured in test No. 107
with $R_g > 20$ MΩ to those measured in test No. 112 with $R_g = 150$ kΩ. The
data shown from test No. 107 were extracted from the oscillograph record-
ing early in the test in order to match arc current and pressure. The
effect of grounding resistance is apparent through the converger and mid-
way through the constrictor. The arc-wall potential difference is reduced
significantly by the higher resistance.
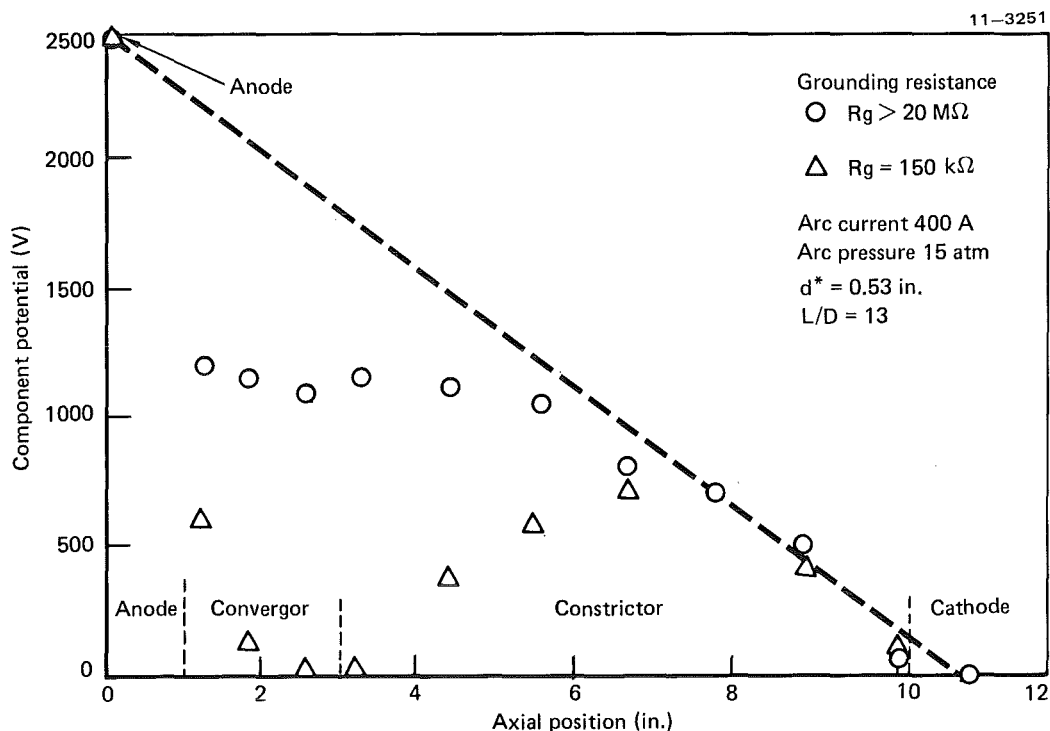
Figure 29 Effect of resistance to ground on component potentials (d* = 0.530)

In test No. 112 with R_g = 150 kΩ, the arc ran for approximately 1.2 s reaching a pressure of 16 atm. The arc current reached a fairly steady level at 400 $\pm$ 50 A. The arc voltage varied from 2350 to 2850 V. The voltage was relatively stable until near the end when apparently the arc blew out on an excursion through the throat. The arc current dropped to about 200 A and the voltage jumped to well over 3000 V at which time there was an external arc on the insulators between the segments. Some of the insulators on the converger were burned, along with the tie-bolt insulator. These were repaired after removing the char. There was no apparent internal damage to the heater. The arc rotation rate initially was 440 rps and then dropped off to about 390 rps at the end of the test.

In test No. 112: (1) the arc current was obviously at a low level since the intensity of the arc was low throughout the test, (2) the arc appeared to be well centered and surrounded by relatively cold gas distinguished by the color blue, and (3) the start-up was apparently of a lower current since the luminosity in the near zero flow phase was almost indistinguishable.

The current decay at the end of test No. 112 was somewhat different in that the diameter of the arc did not appear to diminish appreciably even though the arc current dropped from 450 A to 200 A at a relatively constant pressure of some 16 atm. The intensity of the arc diminished but the diameter remained relatively constant. Toward the end of the test it was observed that there were several arc excursions to the first isolator and this was borne out in the oscillograph trace where the voltage of the first isolator oscillated by about 100 V in the last 0.25 s of the test.

The effect of segment resistance to ground on component potentials when using the smaller nozzle is shown in Fig. 30. The electrode potentials for the two tests are essentially identical but the converger and constrictor entrance potentials are significantly different. The higher grounding resistance reduces the differential between the arc column and the wall and the differential between constrictor segments. Both of these factors should reduce arc shunting and intersegment arcing. The high speed films did not reveal a significant difference between these two tests. The oscillograph recordings were virtually identical except for the segment potentials and occasional intersegment arcing in the low resistance test.
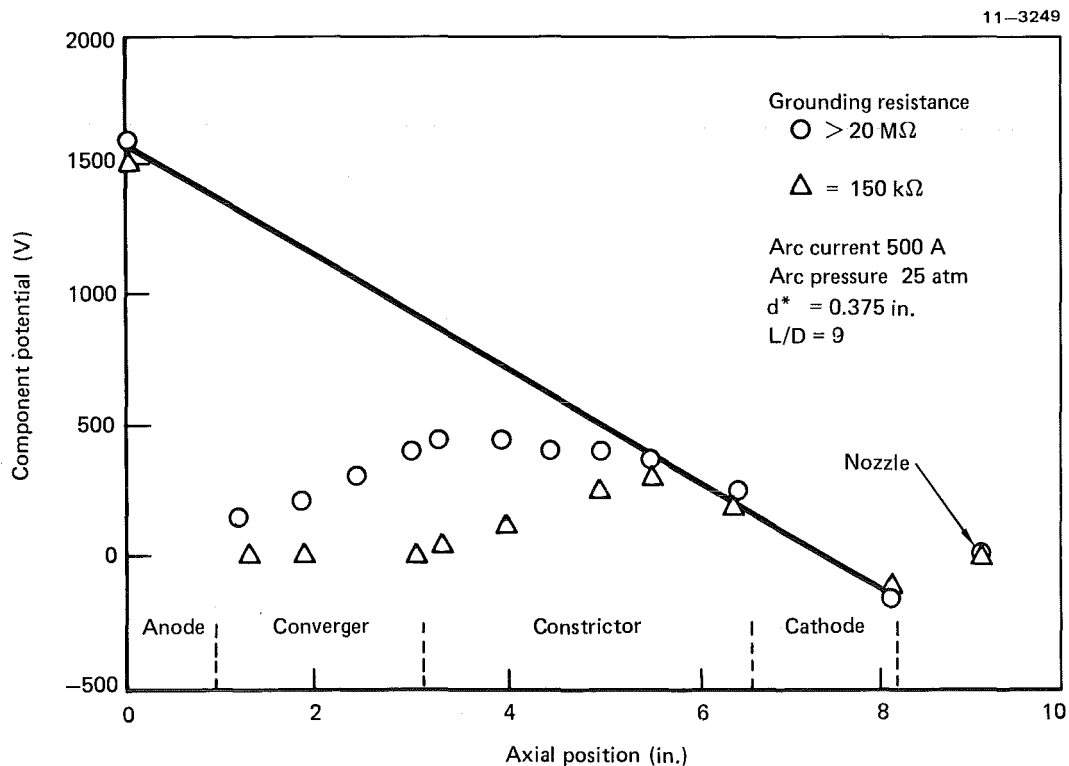
11—3249

Figure 30 Effect of resistance to ground on component potentials (d* = 0.375)

4.3 ARC HEATER GEOMETRY EFFECTS

Two geometry changes were made during these experiments that had a pronounced effect on the arc heater operation. The nozzle area change from 0.11 to 0.22 in.^{2} was discussed earlier with regard to air flow effects. The discussion here will center on the effect of nozzle area on overall stability and resultant hardware conditions after testing. The effects of constrictor length on the arc heater characteristics will also be discussed here. Data for an L/D = 13 were acquired for both nozzle areas. Previous data[5] using the large nozzle with an L/D = 9 will be included to supplement the small nozzle data acquired for that length in this program.

64

4.3.1 Effects of Nozzle Throat Area

The effect of reducing the nozzle area of HIPERARC by a factor of two on the air flow rate can be seen by comparing Fig. 11 to Fig. 10 (Section 4.1.1).   This air flow rate reduction had a pronounced effect on overall arc stability.   Interelectrode segment arc-over became a major problem with the small nozzle.   Significant hardware damage was encountered and alternate plans were required to achieve the desired arc control variations.

Figure 31 shows some of the arc region components after test No. 87 through No. 115 using the larger nozzle and an L/D of 13.   Several variations in test conditions were made with this hardware as shown in Table 2. All major components were in reasonably good condition and there was no significant evidence of intersegment arcing.   The rear electrode (normally the anode) arc tracks were well centered on the toroidal electrode with the only erosion of concern resulting from the tests where it acted as the cathode.   Even that erosion was not severe (Fig. 31a).   The uniform discoloration of the forward quadrant (Fig. 31b) was unique to operation as a cathode for the larger nozzle tests.   Note the scrubbing effect of the tangential injectors indicating some frictional losses in that area.   The converger segments (Fig. 31c) were perfectly clean after testing.   There was no evidence of intersegment arcing.   The photograph of the constrictor segments was overexposed.   Their condition was essentially the same as the converger with a few arc spots near the downstream end.   The entrance to the forward electrode (Fig. 31d) was smooth but discolored indicating no arc-over at the last segment and adequate gas flow at the front slot.   The flared region of the forward electrode (Fig. 31e) contained spiraling arc tracks out to a 2.7 in. diam with some erosion and melt flow near the exit of the smallest diameter section.   The front retard gas maintained a clean region near the electrode-nozzle insulator.   In general, the larger nozzle tests did not significantly damage the arc heater and the arc conditions were predominantly stable.

The initial test series with the smaller nozzle (Test No.'s 116-122) revealed serious arc stability problems and for the first time high speed films of obvious intersegment arcing were acquired.   The arc heater components after test No. 122 are shown in Fig. 32.   The previous arc tracks on the rear
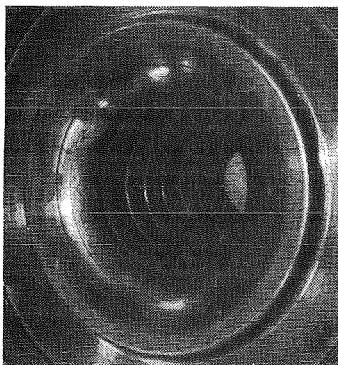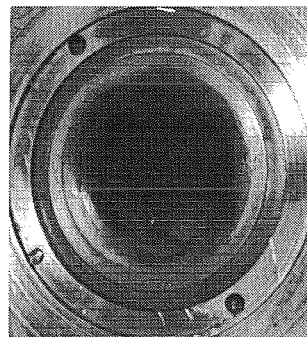
11—3244
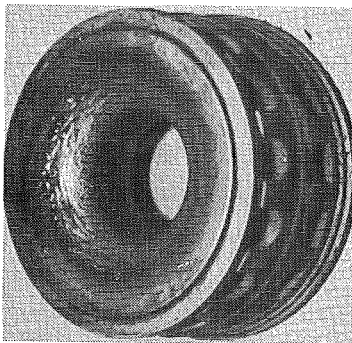
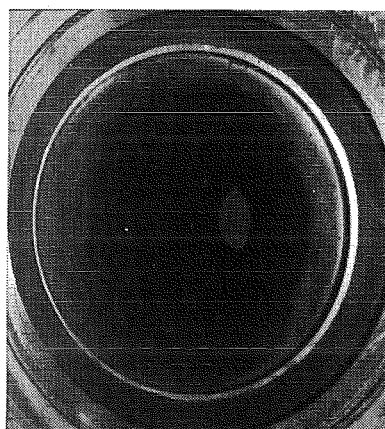a. Rear electrode (rear)
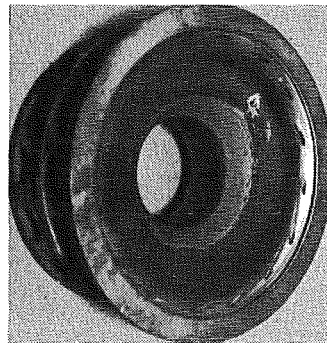
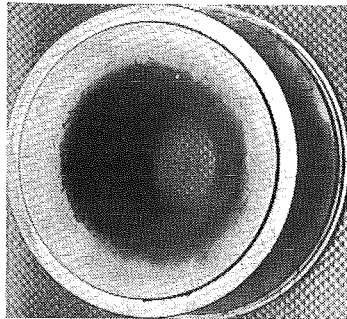b. Rear electrode (fwd)

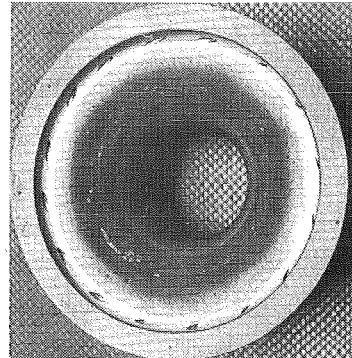c. Converger

d. Front electrode (rear)

e. Front electrode (fwd)
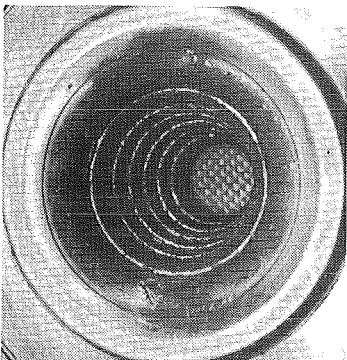
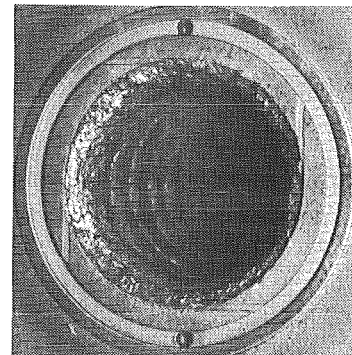Figure 31 HIPERARC after large nozzle tests 87 to 115

11—3245

a. Rear electrode (rear)
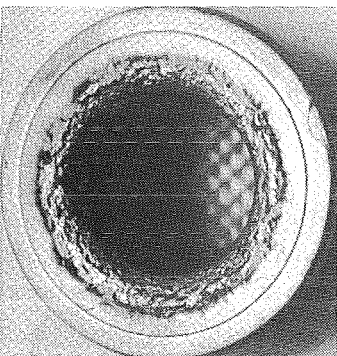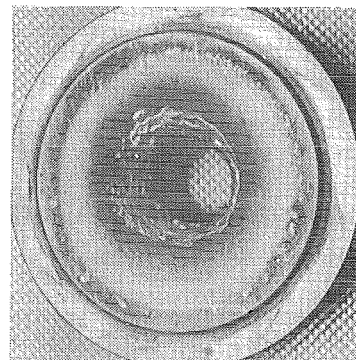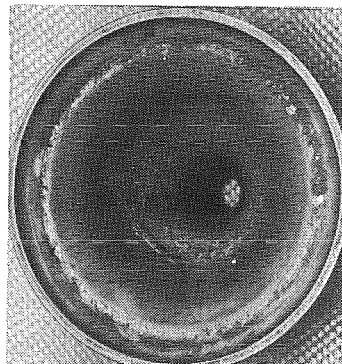
b. Rear electrode (fwd)

c. Converger

d. Constrictor

e. Front electrode (rear)

f. Front electrode (fwd)

g. Nozzle
d* = 0.375 in.

Figure 32 HIPERARC after small nozzle tests 116 to 122

67

face of the anode (Fig. 32a) were covered over with an oxide dust and the
new arc tracks were predominantly forward of the midplane (Fig. 32b)
Significant new tracking occurred at a larger diameter corresponding to
the narrow gap between the rear electrode and the first converger segment.
Scrubbing of the flange wall was increased indicating increased frictional
losses. The arc tracks and edge erosion in the converger segments (Fig. 32c)
were apparent. Tracks on segment one were limited to inside a 2.7 in.
diameter. The disastrous effects of intersegment arcing can be seen at
the entrance to the second pack of constrictor segments (Fig. 32d). Although
these segments were reusable, the roughness of the surfaces enhanced flow
mixing and increased the probability of intersegment arcing. The erosion
in this case was confined to inside the secondary gas injection radius.
The melt flow and arc attachment on the front electrode entrance is seen
in Fig. 32e. The melt flow was even more apparent in the downstream diverg-
ing section of the front electrode (Fig. 32f). With the reduced gas flow
through the front retard, the downstream flange was not kept clean and the
results of arcing between the electrode and nozzle can be seen near the
dirty protrusion. Further evidence of inadequate front retard flow can be
seen on the nozzle (Fig. 32g) and additional solidification of melt flow
is apparent although the throat appears clean.

 A new rear electrode, converger and constrictor were installed for a
second series of tests with the smaller nozzle (test No.'s 123 to 136).
The gas injection radius on the rear electrode was reduced from 1.83 to
1.5 in. The arc termination was moved rearward for most of the tests as
seen in Fig. 33a. The oxide dust coating over these tracks occurred on
the last test of the series when the predominant location was on the for-
ward face (Fig. 33b). The last test (No. 136) encountered severe inter-
segment arcing. Most of the tests in this series had some intersegment
arcing except for those tests with a separately excited field coil on the
rear electrode. Figure 33c shows the results on the converger and Fig. 33d
shows the end of the constrictor where the insulator shield is severely
eroded. The entrance to the forward electrode (Fig. 33e) was also eroded
from the final cascade arc to the entrance corner. The diverging surface
of the electrode appeared normal (Fig. 33f) except for the minor tracking
near the nozzle rim. Some tracks were out to a diameter of 2.75 in.

a. Rear electrode (rear)

b. Rear electrode (fwd)

c. Converger

d. Constrictor

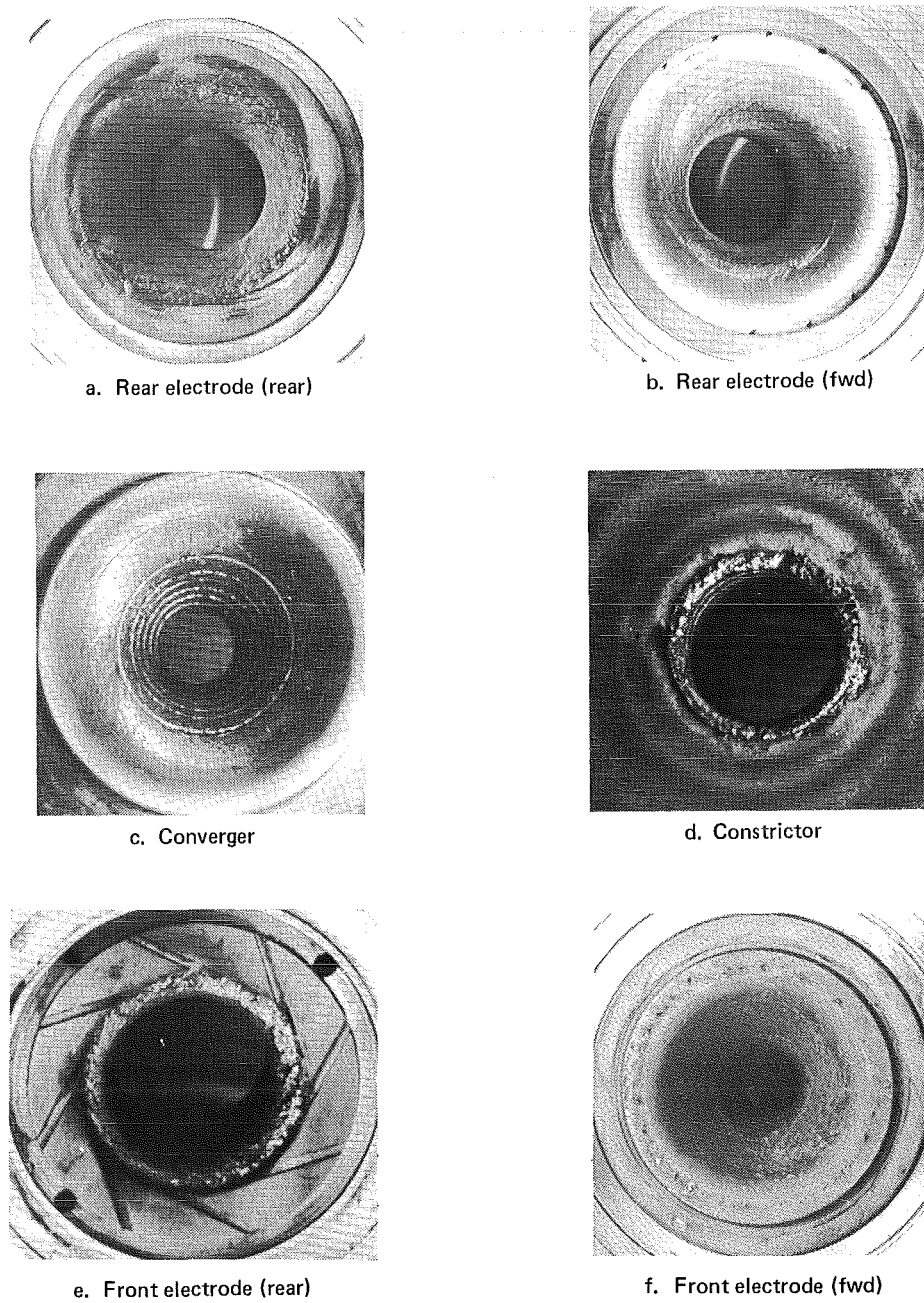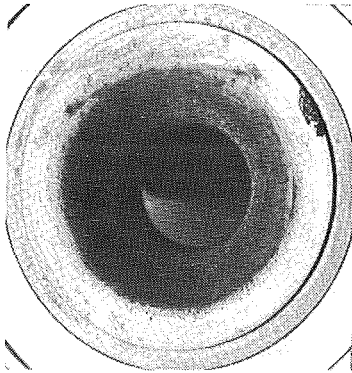e. Front electrode (rear)

f. Front electrode (fwd)

Figure 33 HIPERARC after small nozzle tests 123 to 136

The final test series (No.'s 137-154) was conducted with the smaller nozzle, a reduced constrictor length to increase the gas injection velocity, and a reduced separately excited field coil (after No. 141). The first five tests had minor intersegment arcing but conversion to a separately excited coil and reduction of the coil current to 300 A (No.'s 141-153) virtually eliminated the problem until the 50 atm pressure test (No. 154). Most of the damage shown in Fig. 34 resulted from tests No. 148 and No. 154. Test No. 148 included an arc start with water present from a nozzle O-ring leak and test No. 154 concluded with intersegment arcing. All tests from No. 141 to No. 153, excluding No. 148, were virtually free of problems and damage. The rear electrode (Fig. 34a) was operated as both the anode and cathode in this test series. The same comments made in Section 4.2 apply to this photograph. The severe tracks on the forward face (Fig. 34b) were the result of test No. 148 with water present and a very unstable arc. The predominant arc tracking area was centered on the toroid as desired and the erosion was minimal. The discoloration was greater than in previous tests which is probably due to the higher heat load from higher pressure operation and the reduced field strength slowing arc movement.

The converger (Fig. 34c) damage was predominantly near the exit. All segments remained isolated from each other throughout the converger-constrictor. The front electrode entrance (Fig. 34d) was not damaged but was coated in the entrance with melt flow from the intersegment arcing in test No.'s 137-141, No. 148 and No. 154. The predominant front electrode arc attachment was near the diverger entrance (Fig. 34e). The heavy tracks on the outer rim were the result of arcing to the nozzle and arc-back in the region of the nozzle flange (Fig. 34f). This was the first occurrence of arcing this far out on the nozzle flange.

It should be noted that stability of the arc was greatly enhanced for small nozzle operation by reducing the separately excited field coil strength (reduced Lorentz forces on a spiraling arc) and eleven of the last thirteen tests were free of major instabilities in spite of using previously damaged hardware.
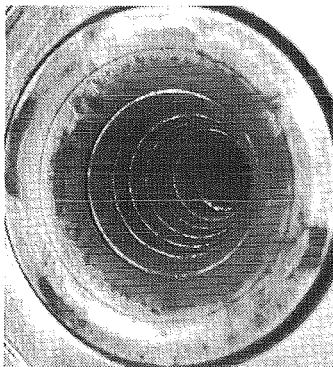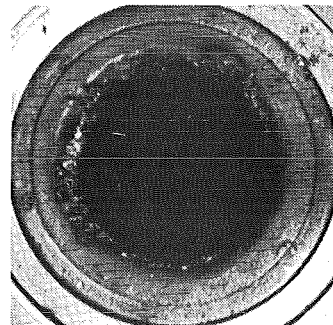
11—3247
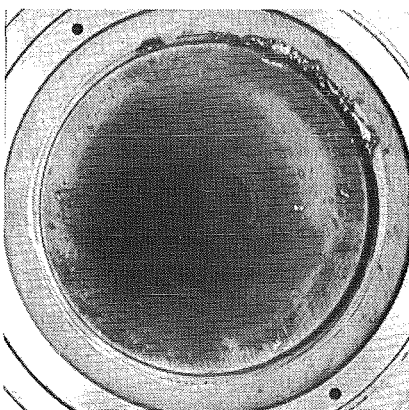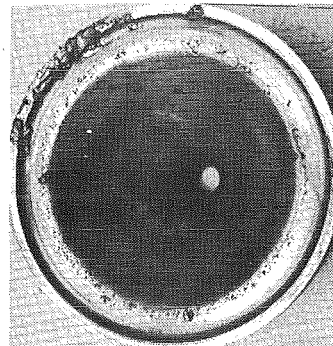

a. Rear electrode (rear)
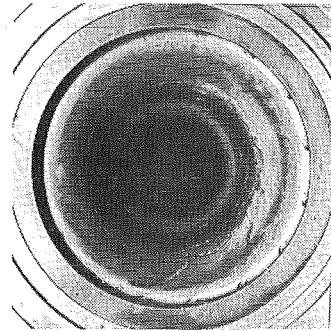
b. Rear electrode (fwd)

c. Converger

d. Front electrode (rear)

e. Front electrode (fwd)

f. Nozzle ($d^* = 0.375$ in.)

Figure 34 HIPERARC after small nozzle tests 137 to 154

4.3.2 Effects of Constrictor Length

Two different constrictor lengths were tested using the smaller nozzle and one using the larger nozzle in these experiments. Previous experiments[5] are herein used to augment those data and provide the second constrictor length for the larger nozzle. The longer assembly consisted of 7 converging segments and 25 constant diameter constrictor segments. The shorter assembly consisted of 7 converging segments and 13 standard segments. The physical length (L) from the midplane of the rear electrode to the end of the arc attachment in the forward electrode was varied from 8.3 to 11.6 in. This corresponds to L/D variations from 9 to 13.

Lengthening the constrictor normally results in higher bulk enthalpy of the gas exiting the nozzle. Thus, for a given pressure the required air flow rate is reduced. This was shown in Figs. 10 and 11 and discussed in Section 4.1.1. Lengthening the constrictor also increases the total arc voltage since the voltage gradient is nearly constant. Figure 15 illustrated the measured arc voltages and they are also discussed in Section 4.1.1.

The effect of constrictor length on rear arc termination location was not significant in the range of these experiments. A comparison of Figs. 33a and 33b shows the primary rear electrode tracks for normal operation are centered on the toroidal midplane for both constrictor lengths. A comparison of Figs. 33f and 33e shows the arc tracks on the forward electrode extended further into the diverger with the long constrictor. This would suggest the positioning is controlled at least partially by the stronger secondary flow with the longer constrictor (31 vs 18 percent).

A composite of the component potentials with two different constrictor lengths is shown in Fig. 35. Higher arc voltage with the longer constrictor is reflected in the converger and constrictor potentials. Since the local column potentials are quite similar, the lower short constrictor potentials illustrate the shrouding effect of the inlet gas. It shows that comparable conduction in the gas surrounding the arc is reached near the constrictor end.
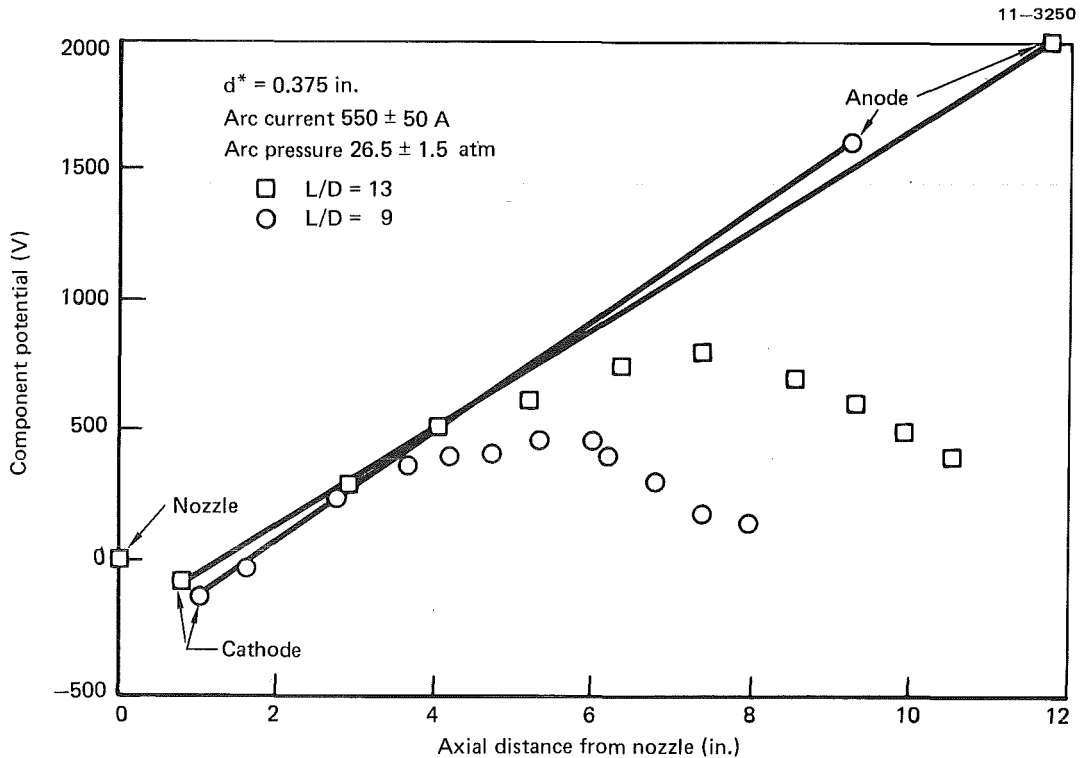
11—3250

Figure 35 Effect of constrictor length on component potentials

The primary advantage of a longer constrictor is increased bulk enthalpy. Studies[3] have shown bulk enthalpy increases can be realized to an L/D of 40. The centerline or core enthalpy is not significantly changed by the constrictor length.[6] If very high gas enthalpies are desired, a short constrictor may be adequate.[5] Selection of the proper constrictor length for the desired performance requires detailed analytical analysis and then experimental validation.

From an arc control standpoint these experiments have shown constrictors that are too short will result in arc blow-through and blow-out and constrictors that are too long can result in insufficient local circulation and intersegment arcing. The arc stability analyses of Cann and Horn[1] and of Shaeffer[6] provide guidelines for constrictor length selection to avoid these instabilities. However, final constrictor length selection must rely on experiments such as those performed here to determine where stable operation can be achieved.

5.0 CONCLUSIONS

Experiments have been conducted using a high performance arc heater to investigate, evaluate and improve arc control at high pressures and currents. The independent and/or semi-independent effects of variations in eight arc control parameters and three geometric factors were documented in high speed motion pictures and on oscillograph records. Table 11 summarizes the effects of the variations made during these experiments on the dominant arc instabilities as gleaned from the data to date.

Table 11 Effects of arc control parameters and geometry

11—3216

Control parameter	Variation	Effect on arc phenomenon					
		Roll over	Spiral	Arc-over	Kinking	Blow thru	Blow out
Arc current (A)	0—830	D	SI	SI	SD	SD	SD
Arc pressure (atm)	0—50	SI	SD	I	D	SI	SI
Air flow rate (lb/s)	0—1.1	SI	SD	I	D	SI	SI
Start ramp time (s)	1—2	D	N	N	D	D	SD
Segment — ground resistance (MΩ)	0.15—20	N	N	D	N	N	N
Spin coil current (A)	300—830	SD	SI	SI	N	I	N
Arc polarity	Std. — Opp.	D	N	N	I	I	I
Primary gas flow (%)	40—83	SI	SD	SD	SD	D	D
Geometric parameter							
Constrictor length/diam.	9—13	D	I	I	I	SD	D
Nozzle throat diam. (in.)	0.375—0.530	SI	SD	SD	SD	SI	SI
Injection radius (in.)	1.5—1.83	D	SI	SI	I	D	D

Key:

I = increased

D = decreased

N = no effect

S = significant effect

The tendency for the rear arc termination to roll over the toroidal electrode and attach to the rear isolator was increased by stronger circulation and both lower arc current and/or lower spin coil current. Increased rear retard gas flow decreased the instability caused by roll-over.

Arc spiraling in the converger region was aggravated by higher arc currents and increased rear electrode spin coil field strength. Both increased the outward radial Lorentz force on the column resulting in large arc spirals in the converger and in many instances intersegment arcing. Arc spiraling was decreased by a higher primary flow rate (higher circulation) whether by an increased total flow or primary flow percentage.

Intersegment arc-over was aggravated by all parameters that increased arc spiraling and/or the arc voltage gradients. Arc-over was initiated by large arc spirals contacting converger segments or column kinks contacting the constrictor.

Arc column kinking was increased at low arc currents and low circulation. Opposite polarity also increased kinking.

Arc blow-through (the nozzle) was aggravated by high gas flow rates and low arc current. Short constrictors and large nozzle areas also increased blow-through. Increased circulation, particularly in the downstream area by higher secondary gas flow, increased arc blow-through.

The occurrence of arc blow-out was generally influenced by the same parameters as blow-through but was more sensitive to low arc currents. The short ramp time was a primary cause of arc blow-out.

Arc stability was improved significantly through reductions in the externally imposed magnetic field on the arc column in the converger. The reduced field strength reduced the outward radial Lorentz force on the arc column and allowed the available radial gas pressure forces to center the arc away from the wall thereby eliminating intersegment arc-over. In addition, the anode was moved rearward on the toroidal electrode to a better cooled region.

Improved gas circulation was demonstrated to have a stabilizing effect on the arc. The larger nozzle tests and the start phase of all tests indicated a higher injection pressure ratio yielded a higher injection velocity, increased circulation and a more stable arc.

In general the arc instabilities downstream of the constrictor
entrance were reduced through an increased arc current and improved circula-
tion. Arc kinking, blow-through and blow-out were all reduced at the higher
current levels. However, high arc currents did aggravate intersegment
arcing in the constrictor under conditions of low circulation and high
rear spin coil field strength.

Further improvements in arc stability and control were realized
through selective changes in local gas flow rates such as the rear and
front retard slots. Reduction of arc attachment to the last segment in
the constrictor was realized by increased front slot flow.

6.0 REFERENCES

1. G. L. Cann and D. D. Horn, The Role of Swirl in Arc Heater Technology, Proceedings of the 26th International Symposium, Instrument Society of America, Seattle, WA, May 1980.

2. D. D. Horn and R. T. Smith, AEDC High Enthalpy Ablation Test (HEAT) Facility, Proceedings of the 24th International Symposium, Instrument Society of America, Albuquerque, NM, May 1978.

3. J. H. Painter and J. F. Shaeffer, High Performance Arc Heater Design, ISA Transactions 18, 1979.

4. W. Winovich and W. C. A. Carlson, The 60 MW Shuttle Interaction Heating Facility, Proceedings of the 25th International Symposium, Instrument Society of America, Anaheim, CA, May 1979.

5. Unpublished HIPERARC data acquired under the McDonnell Douglas Astronautics Company-St. Louis Independent Research and Development, 1979-1980.

6. J. F. Shaeffer, SWIRL ARC - A Model for Swirling, Turbulent Radiative Arc Heater Flowfields, AIAA J. 16, 1978.

7. W. Winovich, On the Equilibrium Sonic-flow Method for Evaluating Electric-Arc Air-Heater Performance, NASA TND-2132, March 1964.

8. J. H. Painter, R. J. Ehmsen, and R. B. Helm, Development of the MDC-200 Air Arc Heater, McDonnell Douglas Report MDC Q0432, July 1972.

9. H. O. Schrade, Electric Arc Discharges in Transverse Magnetic Fields, Part 1, ARL 67-0119, June 1967.

NOMENCLATURE

Symbol	Definition
C	correlation constant, Equation (2)
d_*	nozzle throat diameter (in.)
D	constrictor inside diameter (in.)
h_o	energy balance (bulk) enthalpy (Btu/lb)
L	arc length (in.)
$\dot{m}$	air flow rate (lb/s)
P_i	injector pressure (atm)
P_o	arc pressure (atm)
r	inverse injection pressure ratio
R	resistance (Ω)
v	velocity (ft/s)
V	voltage (volts)
γ	ratio of specific heats

Subscripts

a	arc value
g	wall to ground value
i	injector value
w	wall value